Shape Memory in Crumpled Thin Sheets

Table of Contents

Figures and Tables

Acknowledgments

I would like to express my sincere gratitude to all who helped, advised, and supported me through the process of writing this thesis. First and foremost, I wish to thank my advisor, Dr. Shmuel Rubinstein, for the opportunity to conduct research in his laboratory and for advising me throughout the year. I would also like to thank Omer Gottesman for his help in guiding me through the process of conducting experiments, gathering data, and understanding results in the lab, and for his ready availability to answer and discuss any questions. Third, I wish to extend my gratitude to Dr. Christopher Lombardo, my Associate Director for Undergraduate Studies and a constant source of advice over the past three years. This thesis would not be possible without the guidance and wisdom of these mentors.

I am also deeply grateful to all the members of the SMRLab, for their support and companionship in lab, to the teaching staff of the SEAS Active Learning Lab, to all my professors and teachers in mechanical engineering and SEAS at large, and finally, to all those who helped read, edit, and comment on my drafts.

Chapter 1: Introduction

Memory is one of the defining characteristics of what it means to be human. It consists of the processes and mechanisms of the mind that enable the storage and retrieval of information.[1] It is essential to the way in which we, as humans, act and interact on a daily basis; it allows us to retain knowledge, to develop relationships, to trigger emotions, and to construct our identities. Without the ability to remember, our lives would lack color and vibrancy.

At a more general level, memory refers to the capacity to record information and to recall that same information when prompted; after all, memory is not solely a human characteristic, but also a feature of various other entities, both natural and artificial. Animals in the wild have the capacity to remember, and numerous phenomena in physics, chemistry, biology, and other fields demonstrate hysteresis—a dependence on and remembrance of the history of prior states. Examples include the deformation of rubber bands in mechanics and phase transitions in thermodynamics (Roundy and Rogers, 2013). In addition, memory is a crucial aspect of computers, which require memory both to store long-term information and for short-term functions, in a manner not dissimilar to the memory mechanisms of the human mind.

The storage of memory in a computer uses an ordered system—that is, information is retained in a highly structured and organized manner, with memory retention imposed and assigned in a top-down, pre-instilled manner (Oppenheimer and Witten, 2015). In

[1] http://www.sciencedirect.com/science/article/pii/S0079742108604223

contrast, this thesis focuses on memory retention and information storage in disordered systems. In a physical sense, order and disorder are frequently distinguished by the presence, or lack, of symmetry and organization at a systemic level. With respect to memory, we consider a disordered system not simply as lacking organization in its composition, but also in the ways it stores information. A disordered system does not organize the information to be retained into the existing memory structure; rather, it stores information organically, shaping and reshaping the metastable disordered structure to suit and retain information as needed (Oppenheimer and Witten, 2015). Our goal is to better understand the memory capacity of disordered systems, as well as the mechanisms and methods of these systems that allow for memory retention.

We examine the process of creating a disordered system and the characteristics of disordered systems, and investigate the ways in which each of these factors affects the memory capacity of such a system. We study these goals through the lens of crumpled thin sheets of Mylar, which we use as a model for disordered systems. The phenomenon of crumpled thin sheets is ubiquitous in quotidian life—the image of a sheet of 8.5”x11” paper, blank or lined, crushed into a ball in frustration is perhaps the most obvious archetype. Despite the seemingly trivial nature of this example, a crumpled ball of paper in fact models a tremendously complex and interesting structure. The creases formed on a crumpled thin sheet constitute a disordered system of bistable defects—a network of three-dimensional, physical ‘bits’ that can be popped upward or downward. We study the storage of shape information enabled by these crease ‘bits’ in a crumpled thin sheet, as a proxy for memory retention in disordered systems.

This thesis consists of six chapters. Chapter 2 will provide background information about previous work on the physics of thin crumpled sheets, crease structures, and stress and energy in thin sheets, as well as a discussion of the empirical basis of our model. Chapters 3-5 describe and discuss the phenomenological results of our efforts to characterize the relationship between memory retention and the various factors that define sheet crumpling and crease structures. Finally, Chapter 6 summarizes our empirical understanding of memory retention in disordered systems, and discusses future directions for further study on crumpled thin sheets. The experimental protocols and image analysis methods are described in Appendix A.

Chapter 2: Background

Section 2.1 Previous Work

The study of crumpled thin sheets and their crease structures has a long and varied history, despite the humble nature of their typical appearance in daily life. The dynamics of thin sheets, and the development of sharp points and creases, represent an extraordinarily complex phenomenon (Witten, 2007).

The theoretical foundation of crumpled thin sheets stems from the simpler case of buckling, first analyzed in Euler's *elastica* theory.[2] More recent work has led to the fourth order Föppl-von Kármán equations, governing our understanding of large-scale deformations in membranes and thin, flat plates (Föppl, 1907; von Kármán, 1910; Cerda

[2] http://www.levien.com/phd/elastica_hist.pdf

and Mahadevan, 2003). Individual buckles constitute a form of spontaneous energy focusing, as the elastic energy of deformation concentrates at bent, or deformed, folds (Witten, 2007). These folds are created through the formation of developable cones (d-cones) and stretching ridges, which are point and line singularities, respectively (Cerda and Mahadevan, 1998; Ben Amar and Pomeau, 1997). Multiple d-cone vertices in a single sheet are connected by a stretching ridge between vertices, with flat regions to either side of the ridge (Cerda, et. al., 1997; Witten, 2007). The accumulation of discontinuous buckling events leads to the creation of an array of d-cones, stretching ridges and subridges, and neighboring flat planes, the totality of which produces the crease structures associated with crumpled sheets (Witten, 2007; Pogorelov, 1988). We view crumpling, in short, as the product of repeated buckling.

Repeated crumpling of thin sheets reinforces and rearranges existing creases, and introduces new ridges and d-cones (*Aharoni and Sharon, 2010;* Sultan and Boudaoud, 2006). Existing creases whose localized stresses exceed the yield threshold leave scars on the sheet, creating a historical record of the sheet crumpling (Gottesman, et. al., 2015). The network of accumulated scars created by previous creases constitutes a disordered system. In theory, a sheet can be re-crumpled along the scars of the existing damage, without creating new defects; in reality, however, this is not possible. Though thin sheets have shown a tendency to fold along and/or near existing ridges, limitations of such compression force the creation of new scars and the destruction of some preexisting defects (Sultan and Boudaoud, 2006). In short, repeated crumpling increases the complexity and density of the crease network in a thin sheet.

The total length of the scars in a crease structure has been shown to be a state variable for thin sheets, by Gottesman and Rubinstein, in a paper under preparation; the disordered system of a crumpled sheet can be quantified by a single global quantity, mileage, which varies solely as a function of the number of crumples and the depth of crumple:

$$l = c_1(1-\Delta)\log(1+\frac{c_2+n}{\Delta})$$

where l is mileage, and n and Δ are variables representing the number of crumples and the depth of crumple, respectively. Furthermore, this model of crease length is independent of history and is dependent solely on the state of the system; the increase in total crease length introduced by new crumples is a function of the prior mileage and Δ, with no relationship to the previous number of crumples. It can be expressed as:

$$\delta l = \frac{c_1 c_2(1-\Delta)}{\Delta} e^{-\frac{l}{c_1(1-\Delta)}}$$

Remarkably, we are able to predict the mileage increase per crumple even for an arbitrary sequence of crumpled depths with the above equation for δl. The independence of mileage from the history of prior crumples simplifies the complexity associated with crease structures; Gottesman and Rubinstein suggest that it represents a measure of quantifying the degree of 'crumpledness' of a thin sheet. This model has been shown to hold not only for sheets under axial loading in a cylindrical tube, but also for thin sheets crumpled by hand into a spherical shape.

Crumpled thin sheets have been studied not only in the context of their structure or the dynamics of their creation process, but also in terms of their memory capacity

(Oppenheimer and Witten, 2015). The shapeability of a crumpled sheet, defined as the capacity for deforming and then retaining the deformed shape, stems from the metastability of the disordered crease landscape (Oppenheimer and Witten, 2015; Lobkovsky, et. al., 1995). We model each crease in a crumpled sheet as bistable: it has two discrete, stable configurations (up or down), separated by an energy barrier (Oppenheimer and Witten, 2015). Creases in crumpled sheets can be viewed as an analogue for binary computer bits, with every crease able to store two possible pieces of shape information; each combination of individual crease alignments allows for a discrete, stable sheet configuration, thus producing metastability in the thin sheet (Lobkovsky, et. al., 1995). The relationship between metastability and memory has been extensively studied (Mullin, et. al., 2007; Florijn, et. al., 2014; Silverberg, et. al., 2014).

The shapeability of crumpled sheets differs from shape memory in other systems in a number of key aspects (Oppenheimer and Witten, 2015); it does not require plasticity, unlike pseudoelastic materials, nor is the global deformation of the system simply derived from the superposition of the deformations of each individual element (Huang, et. al., 2010). Instead, by virtue of its disorder, a crumpled thin sheet arrives at a final global shape via the interactions between the deformations of each defect; the local deformations combine but do not necessarily add or subtract in a linear manner to produce the global deformation (Oppenheimer and Witten, 2015). The disorder has further implications, alluded to earlier: though physical systems encode memory by linking a set of original configurations to a set of target configurations, as information to remember, many such systems predetermine the set of target configurations

(Oppenheimer and Witten, 2015). On the other hand, because a crumpled sheet does not undergo the predetermination process and each crease is free to flip to either of its bistable states, the sheet has increased shapeability; this allows it to approximate a wider range of target configurations. The number of possible target configurations is exponential with respect to the number of degrees of freedom of the system, rather than simply proportional to the number of degrees of freedom itself (Oppenheimer and Witten, 2015). It is this memory capacity which we wish to examine empirically in further depth.

Section 2.2 Objectives

Our purpose is to study the relationship between shape memory and crease structure, by furthering the work done by Oppenheimer and Witten and by Gottesman and Rubinstein. We wish to better understand the phenomenon of shapeability in crumpled thin sheets, in an empirical, physical sense, rather than through the uniform triangular lattice model conceptualized by Oppenheimer and Witten; after all, the disordered network of defects in a crumpled sheet cannot be accurately and wholly represented by a prescribed, unvarying lattice. We attempt to establish this relationship between shape memory and crease structure by considering the characteristics of crumpled thin sheets, such as the state variable described in Gottesman.

For our investigation, we follow the procedures used by Gottesman, repeatedly crumpling elastoplastic sheets of Mylar in a cylindrical test tube with a piston. More information on the specific methods and protocols of crumpling can be found in Appendix A. We evaluate the shape memory of a crumpled thin sheet by imposing a cylindrical shape and

determining the ability of the sheet to retain the cylindrical shape after the energy of shape imposition is relaxed. To assess the degree of shape memory retained, we measure the radius of curvature of the crumpled sheet after the force is released.

Our crumpling method is defined by two factors: the depth of crumple and the number of crumples. We measure the former as $\Box$, a dimensionless parameter that we define as the ratio $(h - \delta) / h$, where δ is the crumple depth height, and h is the length of the sheet; $\Box = 1$ represents an uncrumpled sheet and $\Box = 0$ is, in theory, a fully crumpled sheet (in practice, $\Box = 0$ is not a physically possible configuration, since it implies that the sheet has been crumpled to the point that it has no height). The number of crumples, n, is simply the number of times a thin sheet has been compressed in the cylinder. Finally, the state variable, mileage, which we use as a descriptor of the crease structure, is termed l. We refer to a given crumpled sheet by its ($\Box$, n) combination—that is, by the number of crumples and the depth of each crumple that it has experienced. By examining the retained radius of curvature and the crease structures of crumpled thin sheets with different ($\Box$, n) combinations, we seek to better understand the relationship between shape memory and crease structures in crumpled thin sheets, and in turn, the phenomenon of memory retention in disordered systems.

Chapter 3: Memory and Crumpling

Section 3.1 Introduction

At the most basic level, it is essential to understand how different crease structures affect the ability of the crumpled thin sheet to retain shape memory. Given the difficulty in

defining crease structures by quantifying aspects of the structure itself—that is, by the length, density, directionality, or other characteristics of the creases—we distinguish sheets instead by the method of crumpling, using the two factors of Δ and n, as described in Section 2.2. We have an understanding, from the work of Gottesman and Rubinstein, on how the depth of crumple and number of crumples affects the mileage the crease structure, but no work has previously linked the crumpling method or crease structure mileage to memory retention. Thus, in order to understand the behavior of shape memory in crumpled thin sheets, we first seek to understand how varying the depth of crumple and the number of crumples (and thus the mileage of a crumpled thin sheet) affects the retention of shape information.

Section 3.2 Experimental Method and Results

The changes in shape retention in relation to the methods of crumpling are investigated by repeatedly crumpling thin elastoplastic Mylar sheets. We chose three depths of crumple, $\Delta = 0.18$, $\Delta = 0.27$, and $\Delta = 0.45$; for each depth, we crumpled three (or four) Mylar sheets to that depth 20 times, calculating and recording the radius of curvature of the sheet after each crumple (see Appendix A.1 for further information on experimental and computational methodology, and the crumpling protocol). The shape retention of the imposed cylinder increases for the crumpled thin sheets as the number of crumples increases, as we can see from Figure 3-1, which shows the progression of radius retention as the number of crumples increases in each sheet.

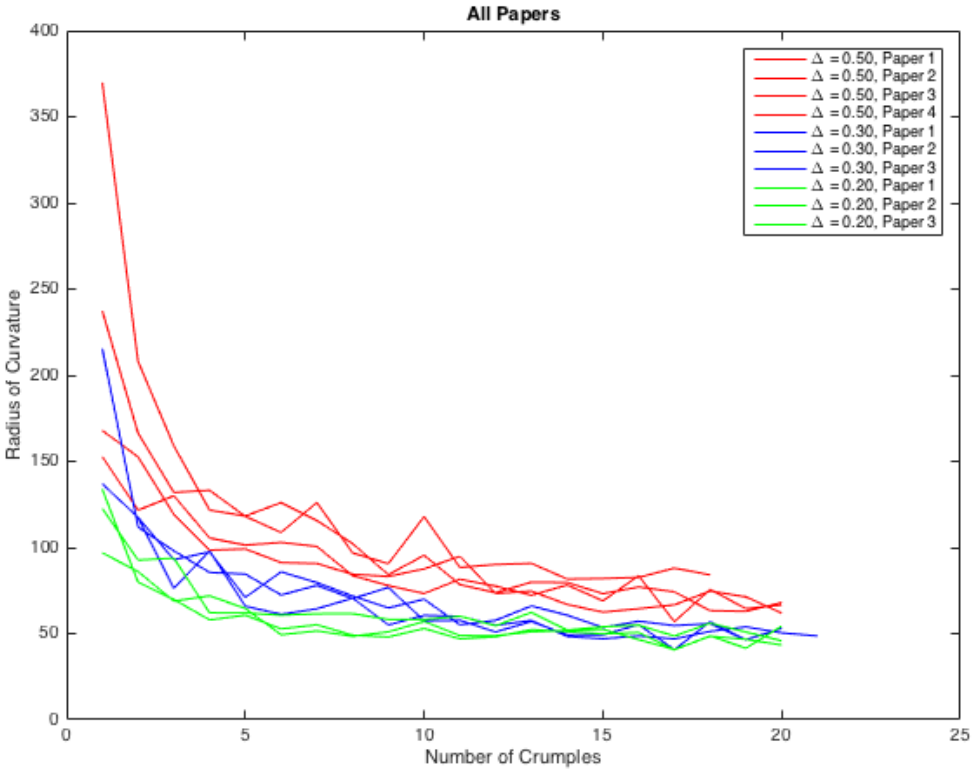

Figure 3-1. The evolution of memory retention. *The radius of curvature retained after each crumple, plotted as a function of the number of crumples, for ten crumpled thin sheets. Different lines of the same color correspond to different sheets crumpled to same values of Δ.*

Perfect memory would produce a radius of 62.0436; this number represents the radius of the cylinder whose shape each sheet attempts to remember via molding, and is calculated using the same methodology for determining the radius of curvature of the sheets of crumpled paper for the above figure (see Appendix A.1-2). A radius of curvature value closer to 62.0436 indicates a greater degree of memory retention.

Section 3.3 Discussion

We can see from Figure 3-1 that a greater number of crumples leads to a decrease in the value for the radius of curvature, though the evolution of the radius of the crumpled thin

sheets is not monotonic. Increases in the retained radius can be observed for each of the ten sheets and are not confined to a particular segment of the *n* values. This can potentially be attributed to the unpredictable and disordered nature of the system under examination; the introduction of new creases and the destruction of previous defects with each new crumple render perfect behavior unlikely. Nevertheless, there is a clear general trend of decreasing radius as *n* increases. It is also clear from Figure 3-1 that the rate of decrease for the radius slows down as *n* becomes progressively larger. This is true for sheets of all three Δ values. We find that a negative exponential function, of the form

$$y = a * e^{-b*x} + c$$

produced a consistent and accurate representation for all ten *r(n)* curves shown in Figure 3-1 (where *r* is the radius of curvature). The negative exponential function is able to capture the decrease in *r* as *n* increases, as well as the slower rate of change of *r* at higher *n* values.

These two trends match our physical understanding of the crumpling process of the Mylar sheets. First, we know that, at a physical level, new crumples often emphasize existing defects, but also that these creases do not allow for a sufficient degree of deformation when a compressive load is applied; the sheet is 'jammed,' and cannot compress further along the previous scars. Instead, new creases must be formed in order to accommodate the necessary deformation. The addition of these new creases, alongside the continued presence of the pre-existing creases, produces a higher number of bistable nodes in the crease structure and thus increases the overall shapeability of the sheet (Oppenheimer and Witten, 2015). At the same time, the amount of new defects created

and the increases in shapeability have an upper limit, since there is less room for new creases as the surface of the thin sheet is gradually filled up with an increasing number of past scars.

The Gottesman model for the evolution of the mileage in crumpled sheets also supports this understanding of the changes in the retained radius. Mileage, which quantifies the total length of creases in a crumpled sheet, is logarithmic with the number of crumples and scales linearly with $(1 - \Delta)$. In other words, it was shown not only that a higher n leads to a larger l value in the crease structure, but also that the incremental changes to l decrease as n increases. This matches the physical understanding outlined above (i.e., that new crumples introduces new creases, but at a decreasing rate) and serves as further confirmation for a possible explanation of the behavior of radius retention in Figure 3-1.

The discussion in the preceding paragraphs is suggestive of a relationship between mileage and the retention of the radius of curvature, given our understanding of the relationships between n and r from Gottesman, and between n and l in Figure 3-1. Establishing such a relationship would provide a possible explanation for how the crease structure, as represented by the total length of its constituent creases, affects the crumpled sheet's ability to retain shape memory. Symbolically, we can see that such a relationship would take the form:

$$r = c_3 * e^{-c_4 * \left(\left(e^{\frac{l}{c_1(1-\Delta)}} - 1 \right) \Delta - c_2 \right)} + c_5$$

based on incorporating our exponential model for radius with the Gottesman function for mileage. However, the relationship between mileage and radius is more complex and

subtle than the derivation shown above; we will see in Chapter 4 that crumpled sheets with the same mileage can demonstrate varying levels of memory retention, perhaps due to differences in crease structure caused by crumple method.

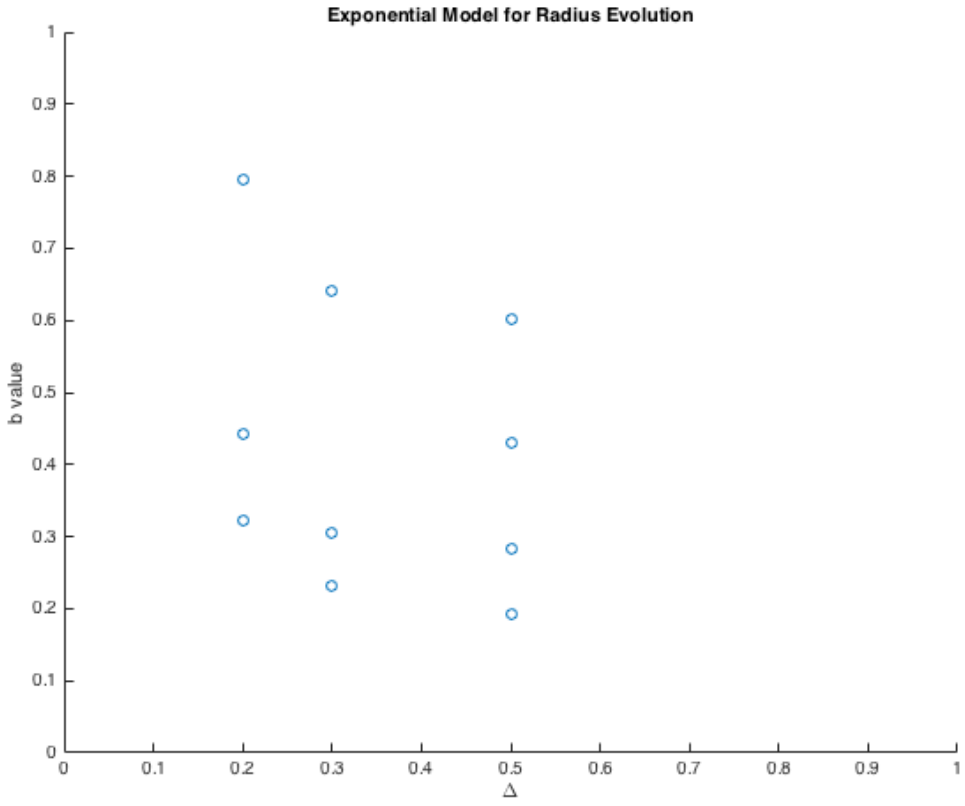

Figure 3-2. Rate of decrease for the evolution of radius. *The growth factor (b) of the exponential model* $y = a*e^{-b*x} + c$ *of the evolution of radius as a function of* Δ. *Each point corresponds with one of the curves in Figure 3-1.*

There are three factors associated with the exponential model that we use to model the behavior of *r(n)* in Figure 3-1: the amplitude factor, *a*; the exponential factor, *b*; and the constant factor, *c*. The amplitude factor does not lend insight into the radius retention, and is thus not included in this discussion. The exponential constant, shown in Figure 3-2, indicates the effect of the number of crumples *n*. The *b*-value displays a wide range for

all three Δ values, but the range is centered on approximately 0.5-0.6 in each case, indicating the rate at which the capacity for shape memory storage in each crumpled sheet is increased (we are unable to explain the variation, except as a result of the imperfect behavior of disordered crease networks). For example, $b = 0.5$ indicates an initial decrease by one-half in the retained radius within the first two to three crumples.

The lack of a discernible pattern to the relationship between the *b*-value and Δ in Figure 3-2 implies that Δ has no effect on the *b*-value of the exponential function; it follows that the rate of increasing memory is independent of the depth of crumple. Instead, the number of crumples is the only variable that our data suggests affects the rate of change of memory retention. It has not been determined, however, if *n* is the sole factor affecting the rate of change of memory retention; it would be worthwhile to consider the rate of radius decrease in a single sheet crumpled to a sequence of different Δ values.

The third factor in the exponential function is the constant, *c*, which effectively defines the lower limit for the *y*-value of the curve as *x* increases. In other words, the *c*-value represents the lowest possible radius of curvature that a crumpled sheet can retain, after a high number of crumples. Figure 3-3 shows that the constant factor varies monotonically with Δ; we can clearly see that the constant factor decreases for smaller values of Δ. In other words, the limit for radius retention is lower in crumpled sheets with deeper crumples.

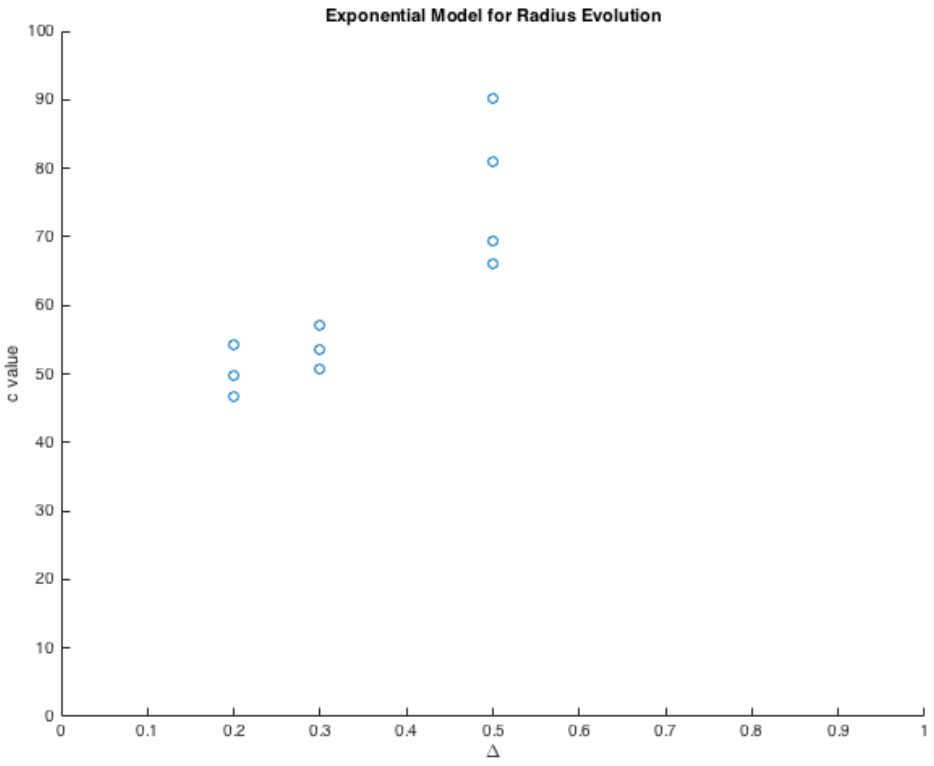

Figure 3-3. Lower limit of radius retention. *The constant factor (c) of the exponential model* $y = a*e^{-b*x} + c$ *of the evolution of radius as a function of* Δ*. Each point corresponds with a curve in Figure 3-1. Note the apparent asymptotic nature of the dataset.*

This matches our intuition, as we expect a deeper crumple to impart greater shape retention memory on a crumpled sheet via a more distributed and heavily imprinted crease structure (see Chapter 5). Since mileage scales with (1 – Δ), we know that a low Δ value corresponds to high total crease length; the same is true for δl, the increase in mileage for a given crumple. The larger total crease length allows for more binary nodes and more shapeability. Thus, we conjecture that the maximum shape retention of a crumpled thin sheet is dependent on the depth to which it was crumpled; deeper crumpling corresponds with greater attainable memory capacity.

While there are an insufficient number of data points in the figure above to construct a reliable curve fit, the relationship between Δ and *c* shown in Figure 3-3 is clearly non-linear; the increase in memory retention does not remain constant from Δ = 0.20 to Δ = 50. The relationship is potentially suggestive of an exponential, suggesting that there may be a lower limit to the *c*-value of the exponential model for different Δ values.

We propose that there exist two maximum limits for memory capacity. First, each crumpled sheet has a local limit for shape retention, which is determined by Δ; the sheet reaches that memory limit at high *n* (this limit is only established for sheets crumpled repeatedly to the same Δ; it is unclear if the limit would exist in sheets crumpled according to an arbitrary sequence of Δ values). Second, we further contend that there exists a global maximum for memory capacity in crumpled thin sheets, independent of Δ and *n*. This limit is absolute, and cannot be exceeded in any crumpled sheet, even for very low Δ and very high *n*. Figure 3-1 supports this conclusion: the tails of the blue and green lines (for Δ = 0.20 and Δ = 0.30, respectively) at high *n* display asymptotes at similar values. While this remains to be quantified in a persuasive manner, the existence of a global maximum would not be surprising; given physical limitations of the sheet, such as size, thickness, plasticity, it is reasonable to posit a maximum possible value for radius retention in a crumpled sheet, and thus a maximum level of shape memory.

Section 3.4 Conclusion

In this chapter, we have explored how the factors that define our crumpling protocol—the number of crumples, *n*, and the depth of each crumple, Δ—affect the crumpled sheet's

ability to retain an imposed radius of curvature. We have shown empirically that the radius decreases as n increases, at an exponential rate; in other words, the memory of the system increases as the number of crumples increases, but at a decreasing rate. We have also shown that the lower limit of the retained radius decreases as the Δ increases, but also at a decreasing rate; we posit that the maximum memory of a given sheet depends on the depth to which it is crumpled, and that there exists a global maximum memory capacity intrinsic to the physical properties and size of the thin sheet. The increase in memory that results from more crumples and/or deeper crumples fits with both our intuition of the physical mechanics of crumpling and the model of mileage established by Gottesman; the same is true for the decreasing rate of radius change.

Chapter 4: Memory and Mileage

Section 4.1 Introduction

We next transition from examining the factors that define the methods of crumpling to exploring the characteristics of the crease structure formed by the aforementioned methods. In this section, we explore the relationship between memory and the mileage of a crease structure. As explained later in Chapter 5, efforts to characterize the physical properties of the crease structure of a crumpled sheet have proven difficult; one exception is mileage, the sum of the length of all the creases (discussed in detail in Section 2.2).

We describe a given crumpled sheet in terms of its (Δ, n) combination—that is, the depth to which it is crumpled and the number of times it is crumpled. Gottesman has shown that mileage, l, can be defined as a function of Δ and n; different sheets with the same (Δ, n)

combination reproducibly have crease structures with the same *l*. The mileage for each (Δ, *n*) combination is shown in Figure 4-1.

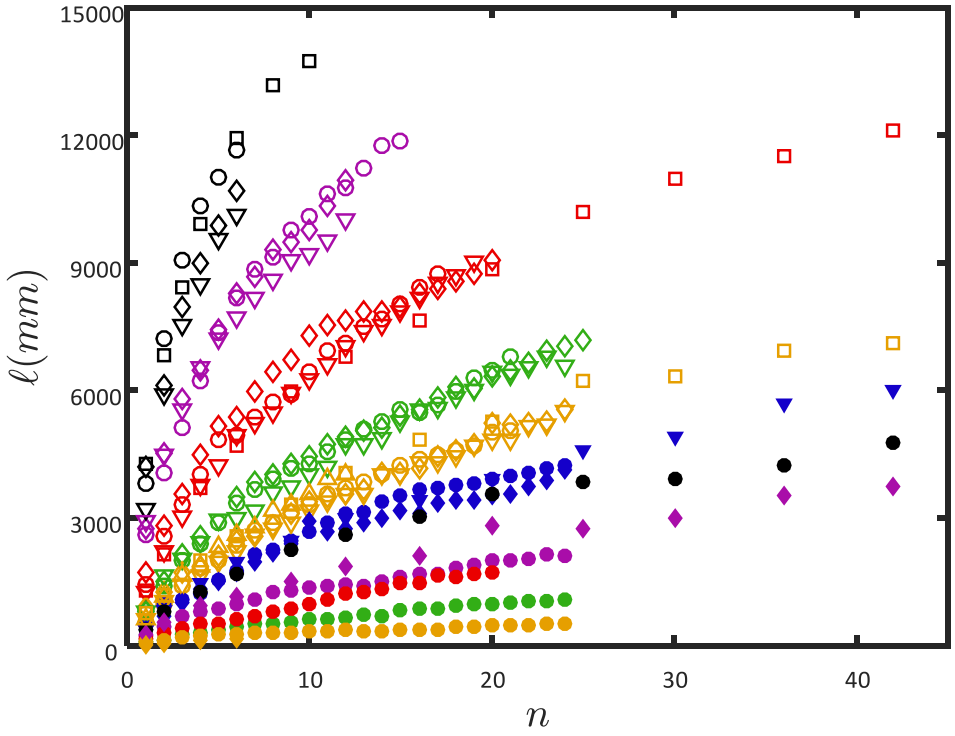

Figure 4-1. Evolution of mileage in crease structures. *Total length of all creases in a crumpled sheet ($l = l_r + l_v$) as a function of the number of crumples for* Δ = *0.045* to Δ = *0.9 (top to bottom). Different markers of the same color represent sheets with the same* Δ *value. Identical color and marker shape indicates the same sheet. Used with permission of Omer Gottesman.*

In Section 3.3, we considered the relationship between the retained radius and the mileage of a crumpled sheet, based on our models of the relationship between *n* and *r*, in Figure 3-1, and between *l* and *n*, in Figure 4-1. We showed that we can theoretically express radius as a double exponential function of mileage, but our model lacked any empirical basis. In addition, our model of *r(n)* in Chapter 3 did provide a modicum of insight about the effect of mileage, since varying *n* while holding Δ constant allows us to examine crease structures with different mileages. We can see that greater mileage

corresponds with increased memory. Both of these modes of analysis, however, ignored differences between crease structures with the same mileage, and the potential effect that these differences may have had on the retention of shape. After all, mileage is only one way of characterizing crease structure, which contains many properties beyond the total sum length of its creases. It is possible that these other factors may also have an effect on memory retention for a crumpled sheet.

In this chapter, we aim to provide a phenomenological description of the relationship between mileage and shape memory. We want to understand whether mileage is an explanatory factor of memory retention in crumpled thin sheets, or if other factors and aspects of crease structure also have an effect on memory retention; quantifying and characterizing the effects of other factors is outside the scope of this section and is explored in greater depth in Chapter 5. In short, we aim to determine if crumpled sheets with the same l, but different (Δ, n) combinations, display the same capacity to retain shape memory.

Section 4.2 Experimental Method and Results

Given our testing protocol and conditions, we determine the Δ value for a crumple by using:

$$\Delta = \left(\frac{D-5}{10*w}\right) * \frac{9}{5}$$

where D is the marking on the test tube to which the sheet was crumpled, and w is the width of the sheet (see Appendix A.1). On the test tube, the markings are in increments of 5; each increment corresponds with 9 millimeters. This allows us to calculate the

approximate *l* for a sheet that has been crumpled to depth Δ a total of *n* times, using the equation for *l* listed in Section 2.1. Using this method of approximation, we choose six mileages and compile a list of *n* and Δ combinations that could produce each chosen *l*.

	1.4k (mm)	*2.4k (mm)*	*4.3k (mm)*	*5.3k (mm)*	*6.5k (mm)*	*8.2k (mm)*
Δ = 0.045			1 (4348)		2 (6630)	3 (8187)
Δ = 0.090		1 (2511)	2 (4143)	3 (5354)	4 (6317)	7 (8399)
Δ = 0.180	1 (1280)	2 (2263)	5 (4314)	7 (5280)	10 (6413)	17 (8267)
Δ = 0.270	2 (1454)	4 (2503)	9 (4295)	13 (5240)	19 (6425)	*33 (8212)*
Δ = 0.360	4 (1404)	6 (2389)	15 (4286)	22 (5255)	34 (6452)	*63 (8277)*
Δ = 0.450	5 (1518)	10 (2504)	25 (4302)	38 (5273)	*62 (6492)*	
Δ = 0.540	7 (1428)	15 (2420)	*43 (4293)*	*69 (5269)*		
Δ = 0.630	11 (1428)	26 (2465)	*82 (4270)*			
Δ = 0.720	19 (1426)	*49 (2425)*				

Table 4-1. Δ and n combinations for the same mileage. *Depth of crumple and number of crumples combinations that produce approximately the same crease mileages. Row headings indicate the Δ value; the first number in each non-heading entry represents an* n *value. The exact mileage produced by the* (Δ, n) *combination for each entry is included in parentheses; each column contains the same mileage. Entries in italics represent* (Δ, n) *combinations that have not been empirically shown to produce the listed mileage.*

Though it is clear from the table above that each *n* and Δ combination does not produce exactly the same *l*, this would be an unreasonable expectation, especially since a non-integer value for *n* is physically impossible to replicate; however, we believe that the *l* values listed are within sufficient proximity to suit our purposes.

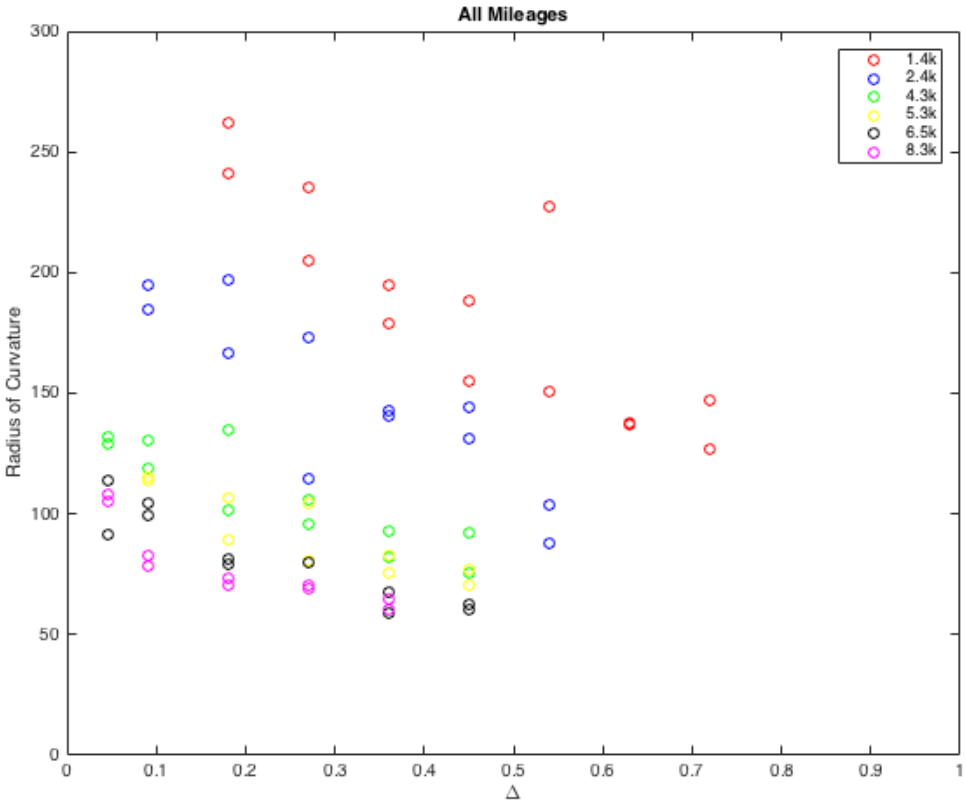

Figure 4-2. Mileage is not the sole factor for memory. *The retained radius of curvature for crumpled thin sheets with the same mileage produced by different* (Δ, n) *combinations, as a function of Δ. Markers of the same color indicate thin sheets with the same mileage of crease defects.*

We crumple two Mylar sheets to each of the (Δ, *n*) combinations listed in the table, according to the protocol described in Appendix A.1, then measure the retained radius of curvature. We compare the retained radii for all sheets with the same mileage, as summarized in Figures 4-2 and 4-3.

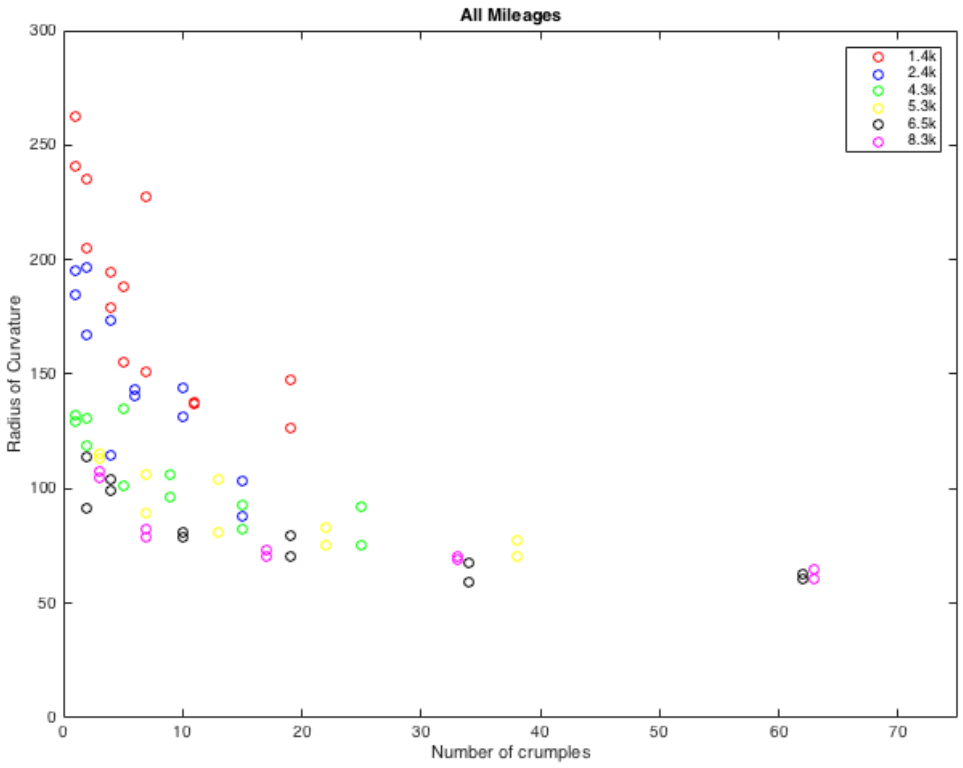

***Figure 4-3. Evolution of radius as a function of* n.** *The retained radius of curvature for crumpled thin sheets with the same mileage produced by different* (Δ, n) *combinations, with radius shown as a function of* n*. Markers of the same color indicate thin sheets with the same mileage of crease defects.*

Section 4.3 Discussion

In Figures 4-2 and 4-3, it is clear that the retained radius decreases as Δ and *n* increase, even for sheets with the same mileage. Figure 4-2 shows that for sheets of the same *l*, the radius decreases as Δ increases; Figure 4-3 shows that the radius decreases as *n* increases. In other words, crease structures produced by a high number of shallow crumples have a greater memory retention capacity than structures created through a low number of deep crumples. Given the presence of these variations in radius even for sheets with the same total crease length, we therefore conclude that mileage cannot provide a full explanation for differences in shape retention on its own. Though mileage does have an impact on

remembering the radius, as shown by the decrease in radius for higher *n* in Figure 3-1, we see clearly in Figures 4-2 and 4-3 that radius retention also varies independently of mileage.

This result is somewhat counter-intuitive, based on our prior understanding of the relationship between crease structures and memory storage. It has previously been shown that the bistability of creases provides the metastability and shapeability of crumpled thin sheets (Oppenheimer and Witten, 2015); therefore, in Chapter 3, we proposed that the increase in memory retention as *n* increased to be a product of the corresponding increase in mileage. More mileage, according to this theory, indicated more creases and thus more degrees of freedom for shape approximation. However, Figure 4-2 shows that this explanation is unsatisfactory. One explanation of the difference in radius retention between crumpled thin sheets with the same *l* is that our foundational assumptions about memory and metastability are incorrect. A more likely option is that crease networks of the same mileage display structural differences that affect the shape memory of the sheet; this is explored in Chapter 5.

Because of the clearer trends in Figure 4-2, we focus on the relation between radius and Δ, for crumpled sheets with a constant mileage; we examine the relationship between radius and Δ for each mileage separately. We find that a linear function, of the form:

$$y = m * x + b$$

best fits the *r(Δ)* curves for the six mileages studied, where *r* is the retained radius of curvature. The only exceptions were for the crumpled thin sheets with *l* = 6.5k (mm) and

l = 8.2k (mm), which more closely mirror exponential functions, rather than linear functions. We are unable to explain this deviation, although a possible factor may be a smaller sample size for those two mileages compared to the other mileages. There are simply fewer (Δ, n) combinations that produce higher mileages than for lower crease mileages. In addition, a greater percentage of the thin sheets for the two mileages were crumpled either to extreme depths (i.e., $\Delta = 0.045$ and $\Delta = 0.09$) or to an extreme number of crumples (i.e., $n = 62$ or $n = 63$).

We conjecture that the physical basis for this overall trend may be the manner in which new creases are formed for crumpled sheets with high Δ and n values. The high number of repetitions of shallow crumpling may serve as a form of 'training': each crumple, even as it creates some new creases, further emphasizes the defects that exist, ingraining memory storage capacity into the crease structure. In addition, the lower amount of compression that occurs in shallower crumples potentially reduces the possibility of deformations that destroy prior crease scars. Keeping and strengthening existing creases could provide a physical basis for increased shape retention.

We consider the factors of the linear model as a function of mileage, focusing on the slope (m) and the y-intercept at $x = 1$, in an attempt to better understand how l affects the relationship between Δ and r; we want to see if different lengths of crease structures have an impact on how the form of the structure affects radius.

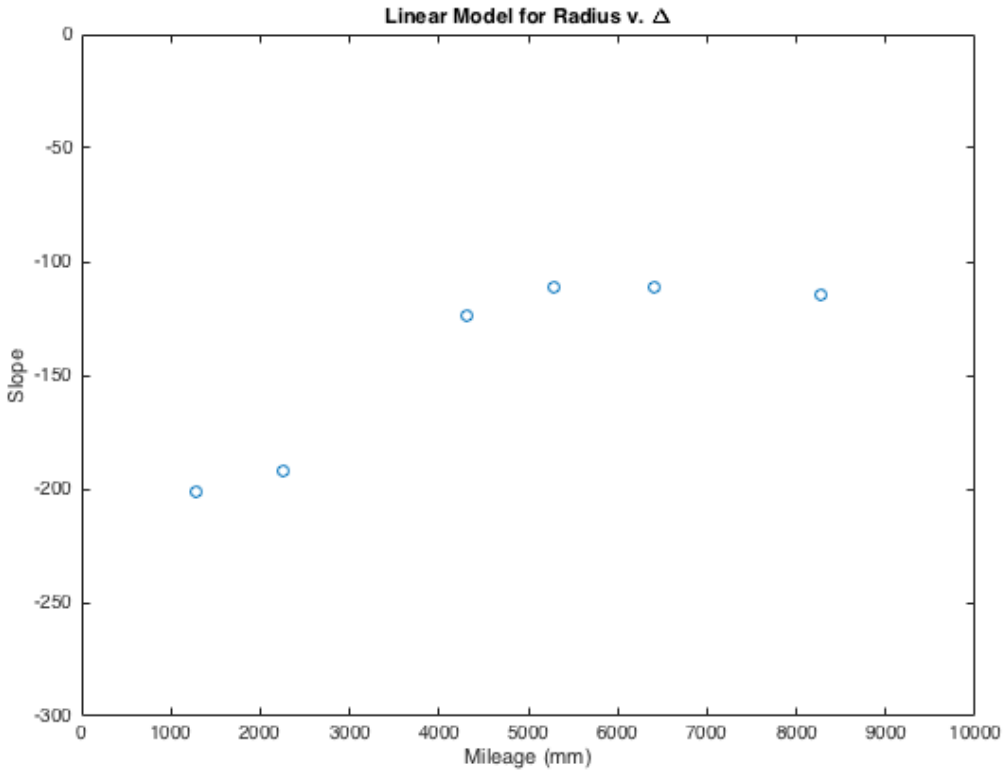

Figure 4-4. Decreasing slope in the linear model of radius retention. *Slope values (m) of the linear model $y = m*x + b$ for radius as a function of Δ given a constant crease mileage. Each point represents a set of points of identical colors in Figure 4-2.*

Examining slope as a function of *l* in Figure 4-4 does not show a sufficient pattern for us to make any conclusions. We do see a general trend towards lower (i.e., more gradual) slopes at higher mileages, though even this claim is not without uncertainty; variations in the scatter may be explainable as a product of differences in the exact *l* of the crumpled sheets or in the *n* value of the crumple. It is also possible that the lower slope for higher mileages can be attributed to the likelihood of greater uniformity in crumpled sheets with higher mileages. More crease length in a crumpled sheet suggests that a greater percentage of the area of the sheet is occupied by creases. At the same time, based on our understanding of the mechanisms and stresses associated with crumpled sheets, there is

little reason to expect that l would have an effect on the relationship between Δ and radius; instead, we leave Figure 4-4 open for interpretation.

We also examine the y-intercept of the linear models at $\Delta = 1$; this value represents the radius of curvature for a sheet crumpled an extremely high number of times at very shallow depths. This would, in theory, give us the lowest possible level of radius retention for crumpled sheets of a given l. These values are calculated by evaluating the models for each mileage at $x = 1$, and are shown in Figure 4-5 as a function of mileage. We can see from Figure 4-5 that our linear model is not perfect and instead breaks down for high Δ values. Two of the six intercept values (for $l = 6.5$k and $l = 8.2$k) are negative; given that the y-coordinates represent the radius of curvature of a crumpled sheet, this does not make sense at a physical level. It is simply not possible for the radius of curvature to be negative. Furthermore, three of the intercept values (for $l = 2.4$k, $l = 4.3$k, and $l = 5.3$k) are under 20; although these values for the radius are not physically impossible, the radius for the cylindrical shape which we impose upon the crumpled thin sheet is greater than 60, rendering a retained radius of 20 rather unlikely.

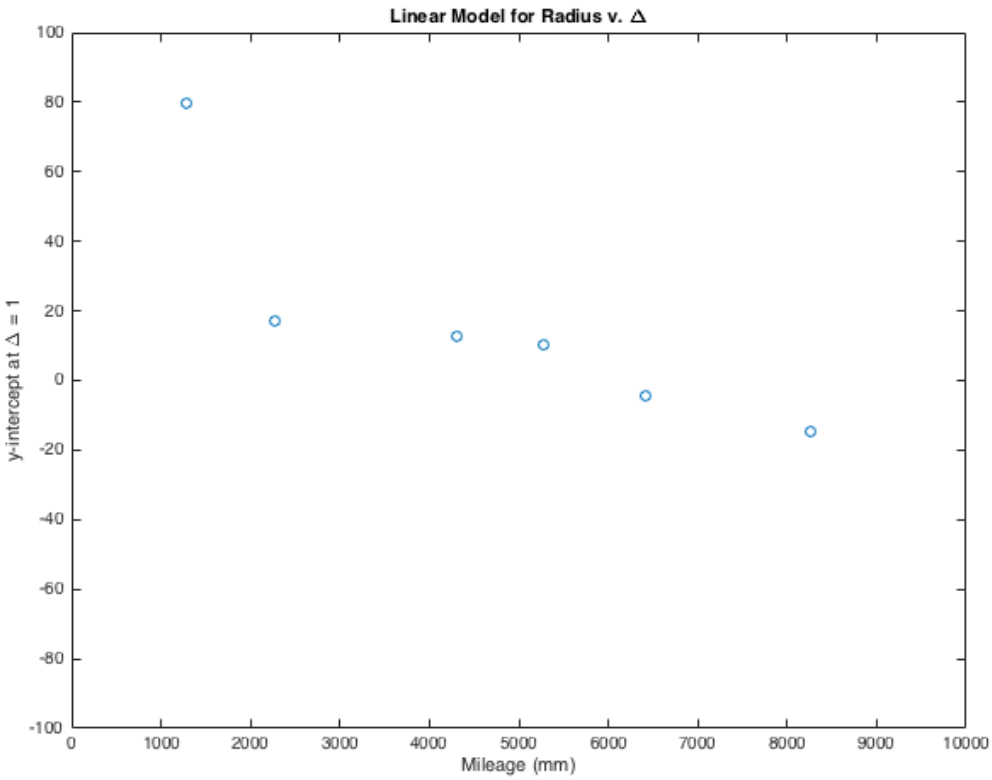

***Figure 4-5. Breakdown of linear model for high* n.** *The y-intercept values at x = 1 of the linear model y = m*x + b for radius as a function of Δ given a constant crease mileage. Each point represents a set of points of identical colors in Figure 4-2. Note that the y-intercept value for l = 6.5k and l = 8.k is negative, which is physically impossible.*

Section 4.4 Uncertainties in Model

The issue that we have identified in the linear model may stem from the nature of the model of crease structure mileage. Due to the logarithmic form of Gottesman's function, a high *n* value is required to reach certain mileages for shallow depths of crumple. For example, as seen in Table 4-1, a sheet must be crumpled 38 times at Δ = 0.45 to reach *l* = 5.3k (mm) in the crease structure and 62 times to reach *l* = 6.5k (mm). While the mathematical model displays no errors for high *n* values, it is unclear if the physical model holds beyond an *n* value of 40, or even beyond 30. The highest number of

crumples for which the l of the crease structure has been measured is $n = 42$, and there have only been 21 measurements for $n > 25$, compared to a few hundred measurements for $n < 25$. A breakdown in the model described by Gottesman when n passes a certain threshold is possible; beyond the threshold, the shallowness of crumple and high number of crumples may combine to create a physical constraint that deviates from the logarithmic model described earlier.

An inconsistency in the logarithmic model for large n would cast doubts on our conclusions regarding the linear model for the decrease in radius as a function of Δ. If the possibility discussed in the previous paragraph regarding the unpredictability of creasing at high n values is true, then it is possible that the linear model also breaks down for high n values and for high Δ values. This would help explain the physically impossible results that we have seen for the linear model when extended to $\Delta = 1$. Finally, the discrepancy here emphasizes that mileage is not sufficient on its own to explain variations in memory retention, both because of questions about how sheets with shallow crumples attain high mileages and because the breakdown of the linear model suggests the possibility of multi-regime behavior in modeling radius as a function of Δ.

Section 4.5 Conclusion

In this section, we have explored the relationship between crease structure and memory. We examined the retained radius of curvature of various crumpled sheets with the same l but different n or Δ values for the crumpling process, and found that the same l does not always correlate with the same memory retention capacity in a crumpled sheet. Instead,

sheets with higher Δ values (and thus shallower crumples) demonstrate a lower radius (and thus more memory) than sheets with the same l but a lower Δ value. This relationship can be modeled by a linear function, though there are doubts of the validity of this model as Δ approaches 1, especially given the physically impossible implications of the model for Δ = 1 and l = 6.5k or l = 8.2k. Thus, we have only established a partial model for the change in radius as a function of the depth of crumple for constant mileage, although the general relationship between lower radii and higher Δ holds true regardless.

That this relationship exists at all demonstrates that mileage is not the full story, even though we consider it a state variable capable of quantifying the 'crumpledness' of a thin sheet. We are unable to predict the radius of curvature of a crumpled sheet using mileage alone; there are other factors that also affect the ability of a crumpled sheet to retain shape information. We conjecture that these differences may be due to variations in crease structure, since the same mileage can be attained by various combinations of n and Δ; it is possible that each (Δ, n) produces crease structures with particular characteristics. For example, a crease structure with many shorter creases as opposed to one with a few longer creases might both have the same l. We next attempt to explore other properties for characterizing crease structures and investigate their relationships with memory.

Chapter 5: Memory and Crease Density

Section 5.1 Introduction

We aim to better understand the relationship between crease structure and memory through the exploration of the factors that describe and define crease structure. Though

Gottesman established mileage as a way to characterize the crease structure of a crumpled sheet, we have seen in Chapter 4 that mileage is not sufficient to explain the behavior of a crumpled sheet in retaining shape information; sheets of the same mileage can display differing degree of radius retention, depending on the method of crumpling (specifically, the n and Δ values associated with the crumpling method). These two variables, however, are only aspects of the crumpling method and are unable to describe the crease structure of a crumpled sheet on their own. Instead, we must quantify other factors that can characterize crease structures.

Possible variables for defining the crease structure of a crumpled sheet include the length of creases (at an individual, rather than total level), the direction of the creases, and the distribution of creases. Attempts to characterize individual crease lengths have so far encountered difficulties in parsing signal noise and differentiating longer creases with multiple intersections from a series of shorter creases. Our unsuccessful efforts to establish a relationship between the directionality of creases and the shape memory of a crumpled sheet can be found in Appendix B.

In this section, we focus on the third characteristic of crease structures: the distribution of crease density. We see in Figure 5-1 that scans of sheets crumpled with different (Δ, n) combinations (but the same mileage) display contrasting patterns; an immediately visible difference is the location of the creases.

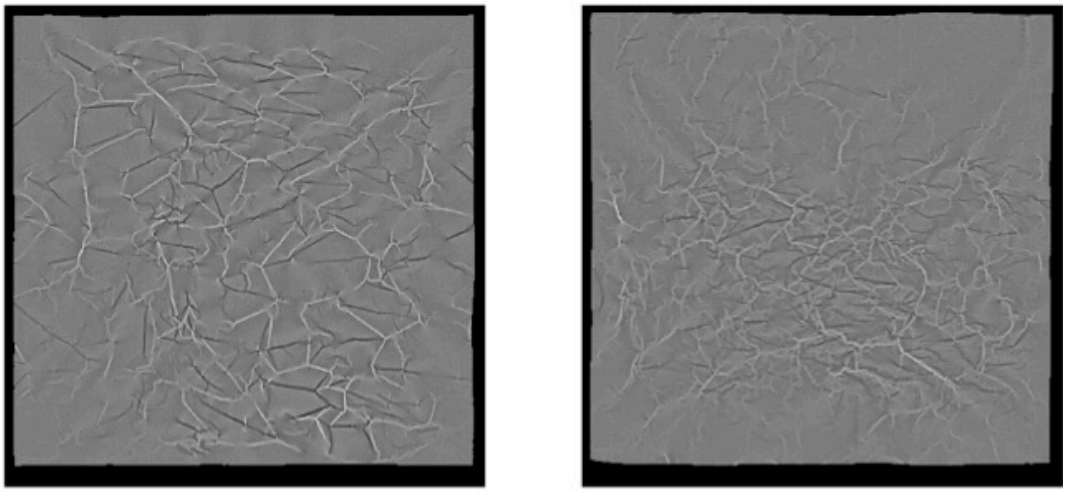

Figure 5-1. Differences in crease structure density for same mileage sheets. *Scans of two representative crumpled thin sheets with approximately the same total damage length (left: ~2511mm; right: ~2465 mm). Left sheet has been crumpled to* $\Delta = 0.09$ *one time (i.e., a single, deep crumple); right sheet has been crumpled to* $\Delta = 0.63$ *twenty-five times (i.e., many, shallow crumples).*

The crease distribution in Figure 5-1a is more evenly distributed, with a few creases in almost every area of the sheet, whereas Figure 5-1b displays a dense concentration of creases along a middle band of the sheet, with few creases in the top half or along the bottom border. These patterns are also seen in other sheets subjected to similar (Δ, n) combinations. We consider the location of scars on a crumpled sheet to be the distribution of creases; we define the density of the crease distribution as a measure of the uniformity of the crease distribution. High density indicates an uneven crease distribution, such that some areas of the crumpled sheet display many creases in a small area; on the other hand, a low density indicates a more even crease distribution, with creases in all areas of the crumpled sheet. We want to determine if this density factor

affects retention of the radius of curvature; we aim to establish a relationship between the distribution of crease locations and the shape memory.

Section 5.2 Experimental Method and Results

We develop a method for quantifying the crease density and the density distribution of a crumpled by partitioning each crumpled sheet scan (as seen in Figure 5-1) into a grid. We find the mileage in each individual grid, then calculate the grid mileage as a percentage of the total mileage of the sheet (see Appendix A.2); we call this the 'area' of the grid. We attempt to characterize the distribution of the individual grid mileages by determining the minimum number of grids needed to attain a threshold percentage of the total grid mileage; we chose to calculate the results for thresholds of 68% and 90%. To do this, we sort the individual grid mileages from largest to smallest, and then sum the mileages until the threshold percentage of total mileage has been reached. We express the number of grids required for this summation as a percentage of the total number of grids in the partition, labeling this percentage ρ. Figure 5-2 shows ρ as a function of Δ for sheets of the same l.

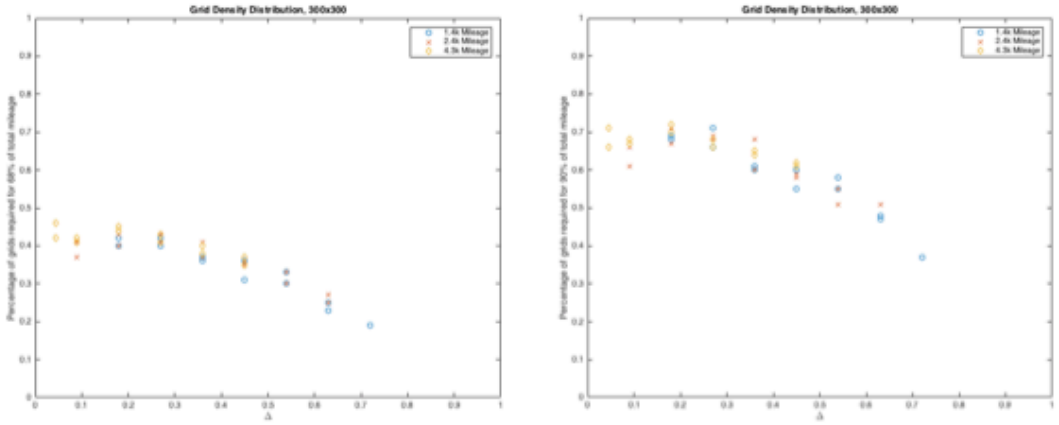

Figure 5-2. Grid density distributions based on mileage threshold. *The percentage of grid partition elements, ρ, needed to attain a threshold percentage of the total mileage of the crease network, as a function of Δ with a grid partition size of 300x300. (a) The evolution of ρ for 68% of total mileage. (b) The evolution of ρ for 90% of total crease mileage.*

The percentage of total grids, ρ, measures the skew in the distribution of grid mileages. A small ρ value indicates a top-heavy distribution with a few areas of the crumpled sheet containing a high percentage of the crease mileage, implying a denser distribution of creases; on the other hand, a large ρ value suggests a more uniform mileage distribution, and thus lower crease density, as there are fewer grids that are heavily populated by defects. Perfect uniformity occurs when ρ has the same value as the threshold percentage of the mileage (i.e., if 68% of the grids account for 68% of the total crease length). A more comprehensive summary of ρ can be seen in Figure 5-3.

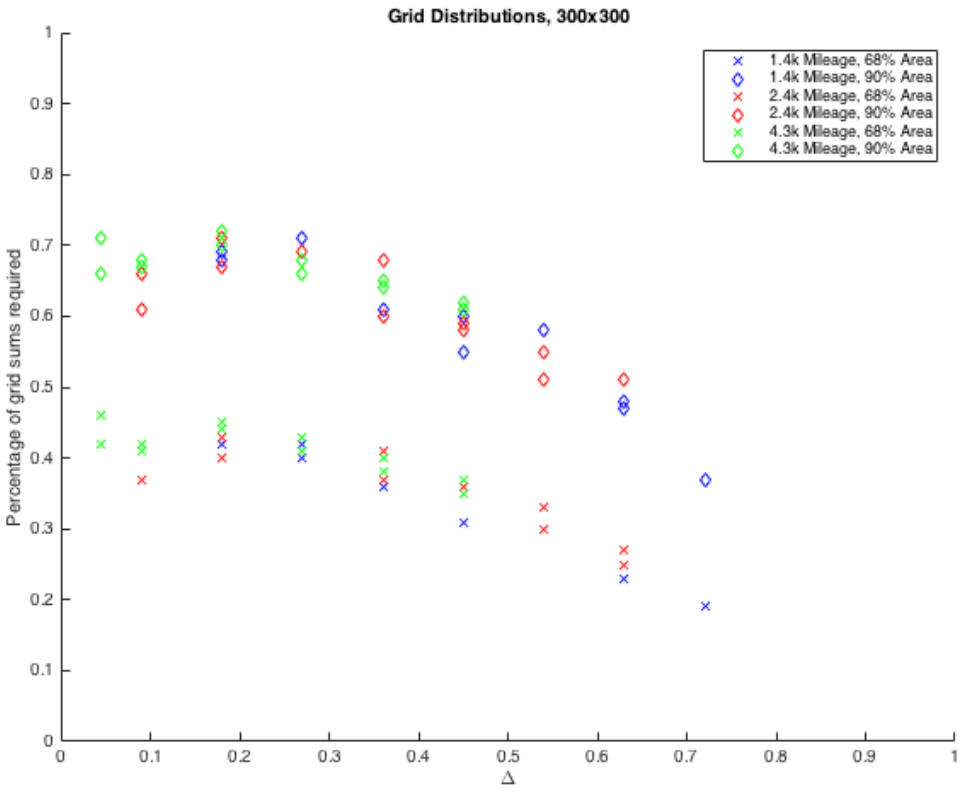

Figure 5-3. Crease distribution tends toward uniformity for deeper creases. *Summary figure for the percentage of 300x300 grids needed to attain the threshold percentage of total mileage in a crumpled thin sheet. Different markers of the same color indicate sheets with the same mileage; identical markers of different colors indicate the same threshold percentage.*

We also investigate ρ as a function of the number of crumples, n, for sheets with the same Δ. The results from our analysis, for the same threshold values of 68% and 90% of the mileage, are shown in Figures 5-4 and 5-5.

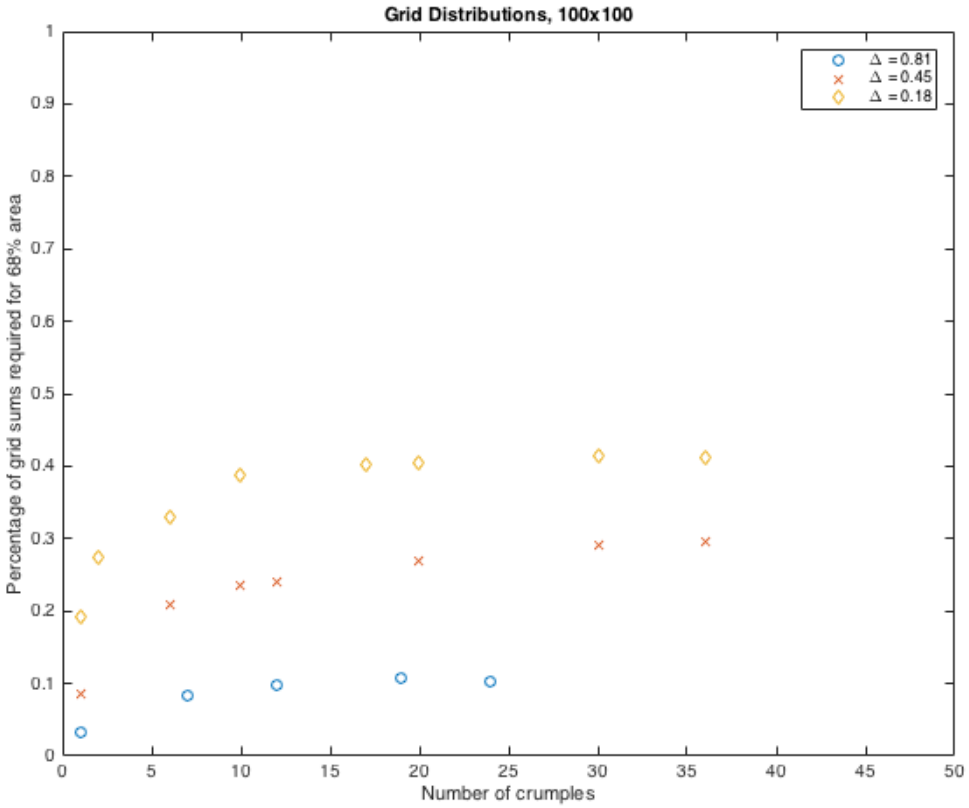

***Figure 5-4. New creases form proportionally for high* n.** *Evolution of crease density,* ρ, *as* n *increases, for Δ values ranging from 0.18 to 0.81. Crease density defined as the percentage of grid elements needed to attain 68% of the total mileage.*

The existence of asymptotes in the evolution of crease density at higher *n* values in Figure 5-4 is immediately apparent. It appears that the *ρ(n)* curve, where *ρ* represents density, has an upper limit that is attained after approximately 10-12 curves. This is confirmed in Figure 5-5, which examines different threshold mileages. Though the value of the upper limit differs in Figures 5-4, 5-5a, and 5-5b depending on the threshold value, the curves in all three figures demonstrate the same asymptotic nature.

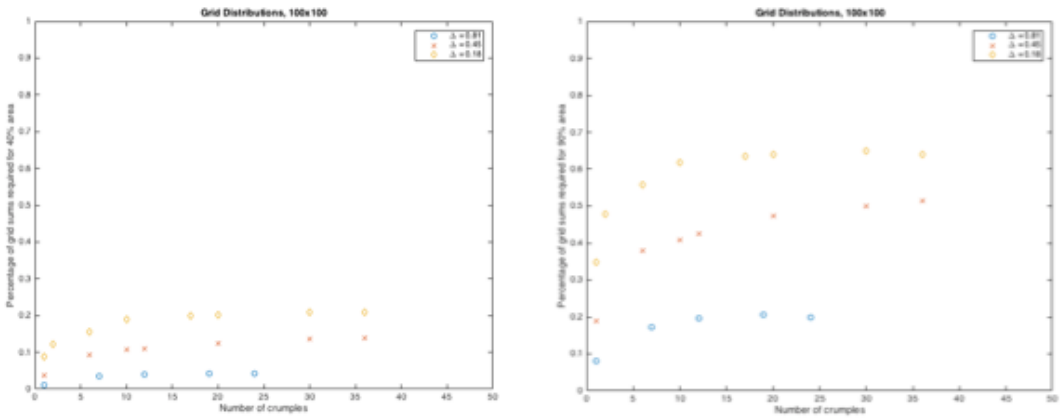

Figure 5-5. Crease density saturates as* n *increases. *Evolution of the crease density distribution as the number of crumples increases, for Δ values ranging from 0.18 to 0.81 with a grid partition size of 100x100. (a) The evolution of* ρ *given a threshold of 40%. (b) The evolution of* ρ *for a threshold of 90%.*

We note that the asymptotes for the ρ of crumpled sheets also vary for different Δ values in Figures 5-4 and 5-5. This difference in ρ is apparent for all n values and for all three threshold percentages. To determine the exact relationship between ρ and Δ, we consider the upper limits of ρ for sheets of different depths of crumples, by calculating the density factor for very high n values. This is shown in Figure 5-6, expressed as a function of Δ.

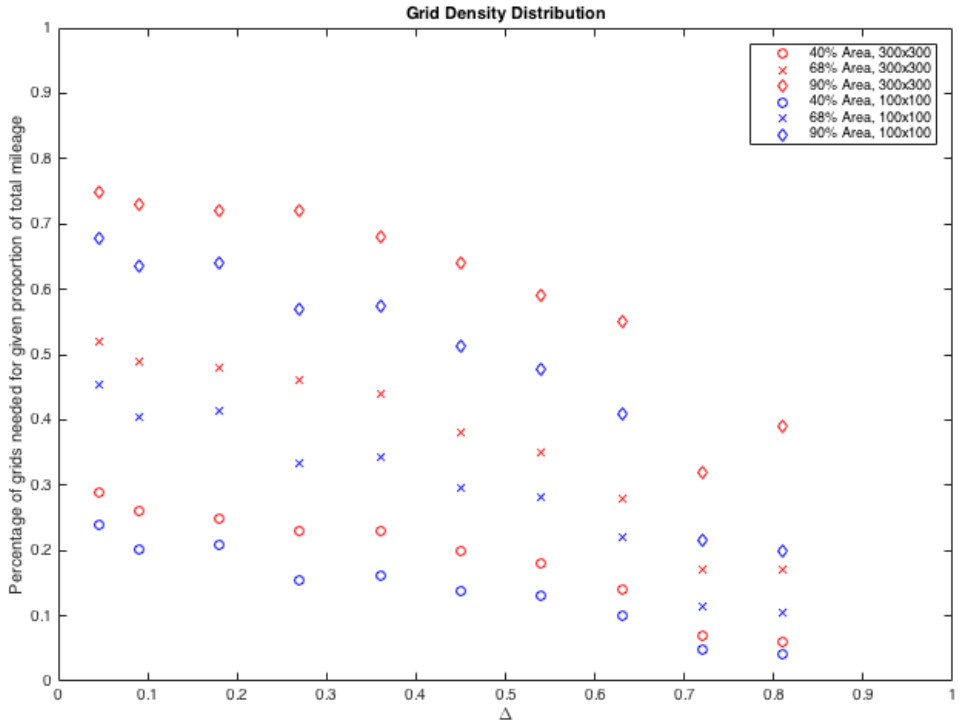

Figure 5-6. Decrease in crease distribution density for shallower crumples. *The upper limit of crease density, ρ_l, defined as the crease density at high* n *values, for Δ values ranging from 0.045 to 0.81. The difference in ρ_l for the two grid sizes is expected.*

The determination of what *n* values constitute a sufficiently high number of crumples is the subject of some ambiguity. Given the scarcity of data available in Figures 5-4 and 5-5, we do not have a means of determining the inflection point for the *ρ(n)* function and thus lack certainty on what *n* values are suitable for evaluating the crease density limit. In addition, our analysis in this regard is further limited by the crease scan images currently available. Based on the set of Gottesman scans, we are able to consider crumpled sheets with *n* values in the range of 30-42 for most of the datapoints in Figure 5-6; however, for crumpled sheets with $\Delta = 0.045$, 0.09, and 0.72, we are only able to consider scans for sheets with $n \leq 20$. This may help to explain the discrepancy at $\Delta = 0.72$.

Section 5.3 Discussion

The evolution of the crease density distribution provides us with a great deal of insight into the formation of new creases in crumpled thin sheets and the development of the crease structure as n increase, and how these affect the memory capacity of thin sheets.

Figures 5-2 and 5-3 demonstrate a remarkably similar pattern for all grid sizes and mileage thresholds: $\rho(\Delta)$ is linear with a negative slope for $\Delta > 0.27$, indicating increasing crease density as the crumple depth becomes shallower and is essentially constant for $\Delta < 0.27$. In the former regime, an increase in the depth of crumple correlates directly with a more uniform crease structure (a higher ρ value indicates greater uniformity in the crease distribution; there are fewer grids with a disproportionately high percentage of the total crease length). Given the linear relationship that we have previously seen between Δ and radius retention in sheets of a given mileage, an obvious parallel can be drawn here with the linear relationship between Δ and crease density, suggesting that greater uniformity in the crease distributed may potentially be associated with lower memory capacity.

However, unlike the relationship in Figure 4-2, the behavior of $\rho(\Delta)$ in Figure 5-3 follows a separate regime for $\Delta < 0.27$. The trend line for the linear regime in Figure 5-2a, extended to $\Delta = 0$, would appear to intercept the y-axis at 0.68, the density level corresponding with full uniformity; similarly, the linear regime in Figure 5-2b extends towards $\rho = 0.90$ at $\Delta = 0$. In reality, the slope of the curve changes at $\rho = 0.27$ and the ρ value for all sheets with $\Delta < 0.27$ remains constant, at a level below 0.68 even for $\Delta \approx 0$ (the same is true in Figure 5-2b, for 90% of the total area). Although the crease density

appears to trend towards full uniformity at $\Delta = 0$, it is never able to attain that distribution. In summary, our data implies that smaller Δ values correlate with a lower grid density and greater distribution uniformity but only to a certain point; at very small Δ values, the crease structure approaches and maintains its density limit, which remains more condensed than a perfectly uniform structure.

The standard deviation of the individual grid crease lengths, as seen in Figure 5-7, confirms these conclusions (though we recognize the limitations of using standard deviation to characterize the non-normal distribution of grid mileages). A lower standard deviation indicates a more uniform distribution, since it suggests less variance between the mileages in individual grids. We see a decrease in standard deviation as Δ decreases, until $\Delta = 0.27$, after which the standard deviation remains constant; this corroborates our result from Figure 5-3 that the uniformity of the crease distribution increases for lower Δ values and then saturates to an upper limit for $\Delta < 0.27$.

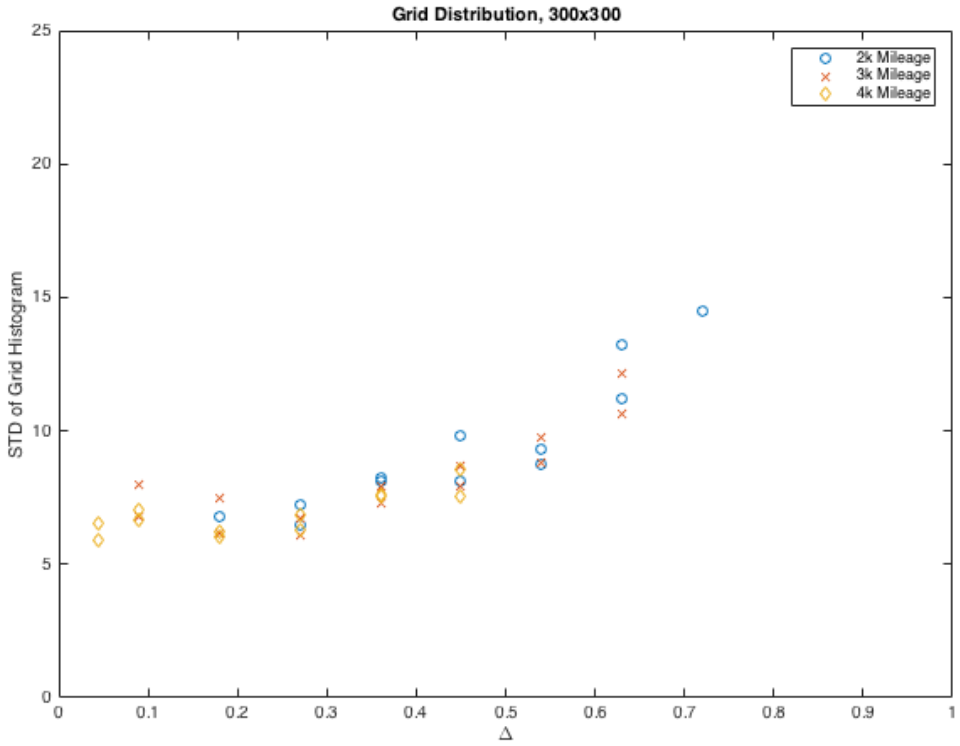

Figure 5-7. Increasing uniformity in crease distribution for deeper crumples. *The standard deviation of the distribution of individual grid element mileages, indicating the degree of variance between grid mileages, for Δ values ranging from 0.045 to 0.72. Different markers of the same color indicate crumpled sheets with the same crease mileage.*

Though the standard deviations shown in Figure 5-7 support our theory about the behavior of new creases, they are unable to explain the surprising convergence of the ρ values for sheets of different mileages but the same Δ in Figure 5-3. The $\rho(\Delta)$ curves for the three mileages in Figure 5-3 all collapse to the same curve, dependent solely on the depth of crumple. For example, the percentage of grids needed for 68% of the mileage in a sheet with l = 1.4k at $\Delta = 0.45$ is approximately the same as the percentage of grids needed for 68% of the mileage in a sheet with l = 4.3k at $\Delta = 0.45$.

A potential explanation for this behavior can be found in examining the behavior of ρ as n increases. Figures 5-4 and 5-5 show that the $\rho(n)$ curve initially increases for smaller n values, before reaching a plateau and remaining constant at an upper density limit (and lower limit of uniformity). We call this density limit ρ_l. Even as the thin sheet is crumpled more and more times, the grid percentage stays at approximately ρ_l, with no further increases. Therefore, we propose that ρ_l is an intrinsic property of the depth of crumple. For a given Δ, the crease structure gradually saturates to its steady-state density, ρ_l, after around 10-12 crumples: the crease structure created by initial crumples is denser than ρ_l (with the crumples distributed unevenly across the structure); re-crumpling introduces new creases that fill up the areas of the crumpled sheet previously lacking in defects, until the density distribution reaches its limit, ρ_l; further creases beyond $n = 10$ no longer alter the crease distribution, but rather contribute to it proportionally. For example, if region A of a sheet has five times the crease length of region B, a new crumple will introduce five times the crease length in region A as compared to region B. This concept of proportional filling of new creases is at once surprising and informative.

In Figure 5-6, we also examine ρ for sheets with high n values, in order to understand the density limit, ρ_l, as a function of Δ. We find that ρ_l decreases linearly with Δ, matching our conclusions from Figure 5-3 regarding the decrease in uniformity for shallower depths of crumple; as Δ approaches 0, ρ_l increases, implying that the steady-state crease distribution is more uniform in thin sheets with deep crumples. The rate of change in Figure 5-6 appears to remain constant, although the grid percentage may taper between $\Delta = 0$ and $\Delta = 0.27$ (our data is inconclusive, due to a small sample size). This matches our

prior findings about the evolution of ρ as Δ approaches 0. We contend that this relationship between ρ_l and Δ may explain the convergence in Figure 5-3. The crumpled sheets in the linear regime of $\rho(\Delta)$ have sufficiently high n values that their crease structures have already reached saturation and thus all display the same density factor of ρ_l; on the other hand, the crumpled sheets of the plateau regime ($\Delta < 0.27$) have not been crumpled enough times to be display saturated crease structures.

However, the precise mechanism that enables shape retention in a crumpled sheet remains unclear. One possibility is Yoshimura buckling, created by a triangular mesh pattern in thin cylinders. We explored the frequency of the diamonds that characterize the Yoshimura pattern, as part of our investigation into the crease density. Further information on Yoshimura buckling can be found in Appendix A.4; results from our analysis of Yoshimura patterns in crumpled sheets can be found in Appendix C.

Section 5.4 Conclusion

In this section, we have found a method for quantifying the crease density distribution of a crumpled sheet, by partitioning the sheet's crease structure into a grid and looking at the number of individual grid mileages necessary to account for a threshold percentage of the total mileage of the sheet. Using this method of characterizing the crease density, we showed that the crease structure, for a given mileage, is more uniform for deeper crumples; the uniformity increases between $\Delta > 0.27$ but remains constant for $\Delta < 0.27$. Further, we showed that the crease density is constant regardless of mileage for a given Δ and a minimum n, which we propose is due to a density limit, ρ_l, which decreases linearly

with Δ. New defects formed from re-crumpling fill less dense areas of the crumpled sheet until ρ_l is reached; after ρ_l is attained, further crumples introduce new creases proportionally in the crease structure such that the density distribution remains constant.

The relationship between Δ and ρ may provide insight into the mechanisms that allow for differing levels of shape retention in sheets with the same mileage. We propose that, at least in the linear regime above Δ = 0.27, less uniformity in the crease distribution (i.e., a narrower distribution density) correlates with greater shape memory. A narrow distribution allows for a high density of creases within a small area, which we argue enables greater radius retention, possibly due to the Yoshimura pattern. We are unable, however, to provide an explanation for the low Δ regime in Figure 5-3 and how the constant density in that regime relates to memory retention. At a more general level, our findings in this section also help us understand the evolution of crease structure and the formation of new creases under re-crumpling.

Chapter 6: Conclusion

Section 6.1 Summary

In this thesis, we have explored the memory storage capabilities and mechanisms of disordered systems, through the lens of analyzing shape memory in crumpled thin sheets. We first sought to develop an understanding of the phenomenology of shape memory, by considering the retention of cylindrical shape in crumpled Mylar sheets, as a function of the mechanisms that create the disordered crease network of a crumpled sheet. We defined the crumpling method by the number of crumples and the depth of crumple. We

then attempted to establish a relationship between the retained radius and the characteristics of the damage network of crumpled sheets.

In Chapter 3, we established an empirical relationship between shape retention in crumpled sheets and the number of times each sheet has been crumpled, given a constant Δ value. The retained radius of curvature decreases exponentially as n increases, at a factor of approximately 0.5. In addition, we conjecture the existence of a lower limit to radius retention for a crumpled thin sheet, even at low Δ and high n values.

In Chapter 4, we examined the relationship between mileage and shape retention, and concluded that mileage is not able to fully explain variances in the capacity of crumpled thin sheets to retain shape. Instead, sheets that acquired the same mileage of total defect length but through different crumpling methods, as defined by the (Δ, n) combination, displayed different levels of memory retention. We found that the retained radius of curvature varied linearly with the depth of crumple for sheets of the same mileage: the retained radius decreased as Δ increased, implying a decrease in memory capacity for deeper crumples.

In Chapter 5, we explored other characteristics of crease structures and their relationships with the retention of radius, since mileage is unable to fully explain shape memory in crumpled sheets. We found that the uniformity of the crease distribution increases as Δ decreases and remains constant (but below perfect uniformity) for $\Delta < 0.27$ in sheets of the same mileage. Moreover, we study the creation of new creases as a function of n,

noting the increase in uniformity at low *n* and the proportional formation of creases at high *n*. We provide a partial explanation for variations in radius retention for sheets of the same mileage, by linking greater crease density to increased radius retention for $\Delta > 0.27$.

Section 6.2 Next Steps

There are a number of analyses that we believe will lend further insight into the relationship between shape memory and crumpled thin sheets. There are other variables that can be used to define the damage networks of crumpled sheets besides the three that we have studied here (the directionality of creases, the density distribution of creases, and the total length of creases). For example, a better understanding of crease lengths and intersections may help clarify the mechanisms by which the crumpled sheet stores shape information.

In addition, more work can be done to better understand the directionality of crease scars in the defect network. Though we have attempted to quantify the relative frequency of creases of certain angles through the use of the Hough transform (see Appendix B), the results from that analysis were inconclusive; it is still possible that crease angles may play a role in memory retention, perhaps through the mechanism of the Yoshimura pattern for cylindrical shapes (see Appendix C). A more thorough analysis of the data generated from the Hough transforms, and/or an exploration of other means for extracting angle data from our crumpled sheet scans, may prove useful.

Third, the density distribution of creases has provided us with a number of interesting results on the formation of new defects in crumpled thin sheets. Although we were unable to establish a full relationship between the density distribution and memory retention, further exploration of these distributions could provide valuable insights into the development of the defect network and the mechanisms for shape information storage. In particular, we wish to better understand the behavior and density of creases for $\Delta < 0.27$.

Section 6.3 Final Thoughts

In summary, we have seen in the previous three chapters that we can relate the storage of shape information in crumpled thin sheets to the two parameters of the crumpling method: both n, the number of crumples, and Δ, the depth of crumple, impact the memory capacity of crumpled thin sheet. We have shown that the crease structure, as represented by the total crease length of a crumpled sheet, also affects the retention of the cylinder's radius, and that mileage alone cannot explain all variations in shape memory. Finally, we have considered the impact of the distribution of scar locations in the crease network, and found that greater uniformity in the crease distribution correlates with lower memory retention, but only at shallower depths of crumple. And we have developed a better understanding of the mechanisms of crease structure development, by noting the proportional formation of new creases for $n > 12$.

Through the lens of crumpled thin sheets, we have sought to better understand the behavior of disordered systems. We have modeled crumpled sheets both as the product of repeated, localized buckling and as a disordered network of binary defects that can be

‘flipped’ up or down. The former has provided us with a foundation for understanding the development of the crease network and the creation of further disorder; the latter has allowed us to appreciate the implications and relevance of our work. Understanding how the shapeability of a sheet changes as the crease network evolves under re-crumpling allows us to draw conclusions about the effects and mechanisms of disorder on the capacity and limitations of memory retention in disordered systems at large. Further afield, a deeper understanding of the evolution of disorder and the development of new damage in the crease network could provide insight into a variety of natural phenomenon, including the evolution of stresses and cracks in earthquake fault networks (Scholz, 2002).

Works Cited

1. Aharoni, H., & Sharon, E. (2010). Direct observation of the temporal and spatial dynamics during crumpling. *Nature materials, **9***, 993-997, doi:10.1038/nmat2893
2. Ballard, D.H. (1981). Generalizing the Hough transform to detect arbitrary shapes. *Pattern Recognition, **13***(2), 111-122. doi:10.1016/0031-3203(81)90009-1
3. Ben Amar, M., & Pomeau, Y. (1997). Crumpled Paper. *Proceedings: Mathematical, Physical and Engineering Sciences, **453***(1959), 729-755.
4. Blair, D.L. & Kudrolli, A. (2005). Geometry of crumpled paper. *Physical Review Letters, **94***(16), 166107. doi:10.1103/PhysRevLett.94.166107
5. Cerda, E., & Mahadevan, L. (1998). Conical surfaces and Crescent Singularities in Crumpled Sheets. *Physical Review Letters, **80***(11), 2358-2361. doi:10.1103/PhysRevLett.80.2358
6. Cerda, E., Chaieb, S., Melo, F., & Mahadevan, L. (1999). Conical dislocations in crumpling. *Nature, **401***, 46-49. doi:10.1038/43395
7. Cerda, E., & Mahadevan L. (2003). Geometry and Physics of Wrinkling. *Physical Review Letters, **90***(7), 074302. doi:10.1103/PhysRevLett.90.074302
8. Chaïeb, S., Melo, F., & G éminard, J. (1998). Experimental study of developable cones. *Physical Review Letters, **80***(11), 2354-57. doi:10.1103/PhysRevLett.80.2354
9. DeBoeuf, S., Katzav, E., Boudaoud, A., Bonn, D., & Adda-Bedia, M. (2013). *Physical Review Letters, **110***(11), 104301. doi:10.1103/PhysRevLett.110.104301
10. DeVries, J. (2005). Research on the Yoshimura buckling pattern of small cylindrical thin walled shells. *Proceedings of the European Conference on Spacecraft Structures*.
11. Florijn, B., Coulais, C., & van Hecke, M. (2014). Programmable Mechanical Metamaterials. *Physical Review Letters, **113***(17), 175503. doi:10.1103/PhysRevLett.113.175503
12. Föppl, A. (1907) *Vorlesungen uber Technische Mechanik.* Lepzig: B.G. Teubner. (cross-referenced from other sources)
13. Gottesman, O., Efrati, E. & Rubinstein, S. M. (2015). Furrows in the wake of propagating d-cones. *Nature communications, **6***. doi:10.1038/ncomms8232
14. Hoff, N. J. (1966). The perplexing behavior of thin circular cylindrical shells in axial compression. *Second Theodore von Kármán Memorial Lecture of the Israel Society of Aeronautical Sciences*.
15. Huang, W.M., Ding, Z., Wang, C.C., Wei, J., Zhao, Y., & Purnawali, H. (2010). Shape memory materials. *Materials Today, **13***(7-8), 54-61. doi:10.1016/S1369-7021(10)70128-0
16. Lobkovsky, A., Gentges, S., Li, H., Morse, D. & Witten, T. (1995). Scaling properties of stretching ridges in a crumpled elastic sheet. *Science, **270***(5241), 1482-85.

17. Mullin, T., Deschanel, S., Bertoldi, K., & Boyce, M.C. (2007). Pattern Transformation Triggered by Deformation. *Physical Review Letters,* ***99***(8), 084301. doi:10.1103/PhysRevLett.99.084301
18. Oppenheimer, N. & Witten, T. (2015). Shapeable sheet without plastic deformation. *Physical Review E,* ***92***(5), 052401. doi:10.1103/PhysRevE.92.052401
19. Pogorelov, A. V. (1988). *Bendings of Surfaces and Stability of Shells* (J.R. Schulenberger, Trans.). Providence, R.I.: American Mathematical Society.
20. Roundy, D. & Rogers, M. (2013). Exploring the thermodynamics of a rubber band. *American Journal of Physics,* ***8***, 20-23. doi:10.1119/1.4757908
21. Scholz, C. H. (2002). *The mechanics of earthquakes and faulting*. Cambridge [England]; New York: Cambridge University Press.
22. Silverberg, J.L., Evans, A.A., McLeod, L., Hayward, R.C., Hull, T., Santangelo, C.D., & Cohen, I. (2014) Using origami design principles to fold reprogrammable mechanical metamaterials. *Science,* ***345***(6197), 647-50. doi:10.1126/science.1252876
23. Sultan, E. & Boudaoud, A. (2006). Statistics of crumpled paper. *Physical Review Letters,* ***96***(13), 136103. doi:10.1103/PhysRevLett.96.136103
24. Tarnai, T. (1994). Folding of uniform plane tessellations. *Origami Science and Art: Proceedings of the Second International Meeting of Origami Science and Scientific Origami*, 83-91.
25. von Kármán, T. (1910) Festigkeitsproblem im Maschinenbau. *Encyk. der Mathematische Wissenschaften, VI*, 311-385 (cross-referenced from other sources)
26. Witten, T. (2007). Stress focusing in elastic sheets. *Reviews of Modern Physics,* ***79***(2), 643-675. doi:10.1103/RevModPhys.79.643
27. Yoshimura, Y. (1955). *On the Mechanism of Buckling of a Circular Cylindrical Shell Under Axial Compression* [Memorandum]. Washington, D.C.: National Advisory Committee for Aeronautics.

Appendix A: Methods

Section A.1 Crumpling Protocols

The foundational block of our experiments was our crumpling methodology, by which we introduce damage to square Mylar sheets, of thickness 30 micrometers. In Chapter 3, we use Mylar sheets with side length 9 centimeters; in Chapters 4 and 5, we examine sheets of side length 10 centimeters. We roll up the sheet and insert it into a cylindrical test tube, with an acrylic piece placed at the conical end of the test tube to provide a flat surface for the sheet to rest on. The sheet is allowed to relax and expand to the full diameter of the test tube, which is 27 millimeters. The marking on the side of the test tube allow us to control the crumple depth; the markings are incremented by units of 5, corresponding to 9 millimeters between markings. We then use a metal post as a piston to compress the sheet downwards, such that it is crumpled vertically while being constrained radially by the test tube (DeBoeuf, et. al., 2013). After we compress the Mylar sheet to the desired depth, we remove first the post, then the crumpled sheet.

The steps taken after each crumple differ based on the experiment. For determining the evolution of the radius of curvature as a function of the number of crumples in Chapter 3, we place the crumpled sheet on a stand to be photographed after each crumple (with the height of the stand determined by the camera height). For the crumpled sheets used in Chapter 4, we press flat the sheet after each crumple, in order to minimize biases for the next crumple, but only take a photograph after crumpling the sheet the desired number of times. Finally, the images used in Chapter 5 were taken from profilometer scans of crumpled sheets. For more information on the calculation of the radius of curvature from

a crumpled sheet scan and other image analysis of the scan data, see Appendix A.2; for more information on the laser profilometer, see Appendix A.3.

Section A.2 Image and Data Analysis

This section is broken up into three parts: first, a discussion about the methods used to calculate the radii of curvature for the crumpled sheets analyzed in the Chapter 3 and 4; and second, a discussion on the methods for investigating crease density and density distributions in Chapter 5; and third, a discussion of the Hough transform.

In order to calculate the radii of curvature for a crumpled sheet, we first determine the edge of the sheet in the axial direction of the imposed cylinder, as shown in the photograph in Figure A-1(a). Using ImageJ, we use the 'Enhance Contrast' and 'Smooth' functions to accentuate the distinction between the edge of a crumpled thin sheet and the background, and then utilize the 'Find Edges' function to determine the exact edge boundaries. We import the edge image produced by ImageJ, shown in Figure A-1(b), into MATLAB where we use the 'edge' function to further emphasize the crumpled sheet edge; we also the 'medfilt2' function to filter out noise. The results of this script can be seen in Figure A-1(c). Finally, we sharpen our data in MATLAB by eliminating other edges detected in the above process and any noise, as shown in Figure A-1(d). Finally, we use a MATLAB script to calculate the radius of curvature of the points shown in Figure A-1(d) by looking at the distance between each set of adjacent points.

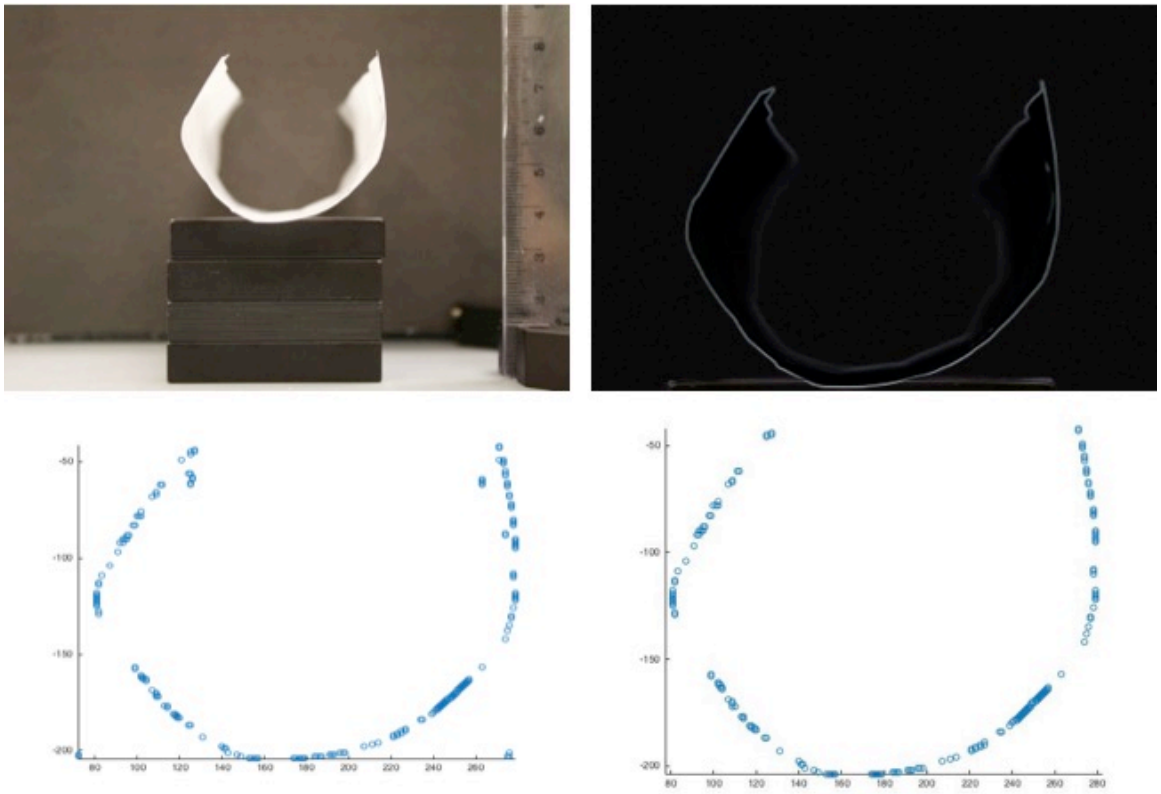

Figure A-1. Edge detection of crumpled sheet radius. *The four steps of determining the edge of a crumpled thin sheet are shown here. (a) The photograph of the crumpled thin sheet, after the energy of shape imposition has been released. The height of the stand for the sheet is determined by the camera dimensions. (b) The initial edge detection of the crumped sheet photograph in ImageJ, after enhancement and smoothing processing. (c) The edges from Figure A-1(b), as viewed in MATLAB. (d) The final edge image, after filtration of noise and non-relevant edge in MATALB. The datapoints in Figure A-1(d) are used to calculate the radius of curvature retained by the crumpled sheet.*

In Chapter 5 and Appendix B, we examine the pattern of crease networks on the crumpled thin sheets. For these investigations, we used the profilometer scans of crumpled thin sheets created by Omer Gottesman (see Appendix A.3). We analyze these scans in two manners: first, using an image dilation and filtration script to highlight the creases in the scanned sheet, with valleys and ridges distinguished on the output image; second, by filtering once to show the 'valley' defects and filtering a second time to show the 'ridge' defects, then combining the two filtered images, displaying all defects with no

distinction between valleys and ridges. The former method was used primarily in our investigation of the Yoshimura pattern in crumpled thin sheets (see Appendix C); the latter was utilized in both our analysis of the directionality of crease defects (see Appendix B) and our examination of the crease network density distribution (Chapter 5).

To quantify the density distribution, we divide the sheet scan in two manners, by a horizontal partition and by a grid partition, and examine the mileage in each individual partition element, relative to the total mileage of the sheet. This is done in MATLAB, using the second method of investigating the crease network (with no distinction between ridges and valleys). For the grid partition, we tested grid sizes ranging from 10x10 (90000 total grids) to 500x500 (36 total grids), given an image size of 3000x3000 (double), from which we decided that grid sizes of 100x100 and 300x300, which produce 900 and 100 total grids respectively, are best able to both capture the distribution shape and are sufficiently large to be insightful. For each partition element, we calculate the mileage of that element by summing across the element area.

The distributions of these mileage densities are then characterized in a number of ways. First, we normalize the total sum of the individual grid mileages, then determine the least number of grids required to attain a given percentage of the total mileage. We used three percentages—40%, 68%, and 90% of the mileage. To do this, we sum the mileage contained in the individual grids, starting from the grid with the highest mileage, until our sum reached the requisite percentage of the total mileage. We then calculate the number

of grids used in that sum as a percentage of the total number of grids in the partition. The same analysis is done for the horizontal partition as well.

Second, we consider the standard deviation of the distribution of grid mileages in a given sheet; this is done with the 'std' function in MATLAB. Third, we consider the histograms of the grid mileages, for both grid sizes; a representative histogram is shown in Figure A-2(a). Fourth, we plot the mileage of each horizontal partition as a function of height, as shown in Figure A-2(b). These four modes of analysis provide the basis for our understanding of the crease density distribution.

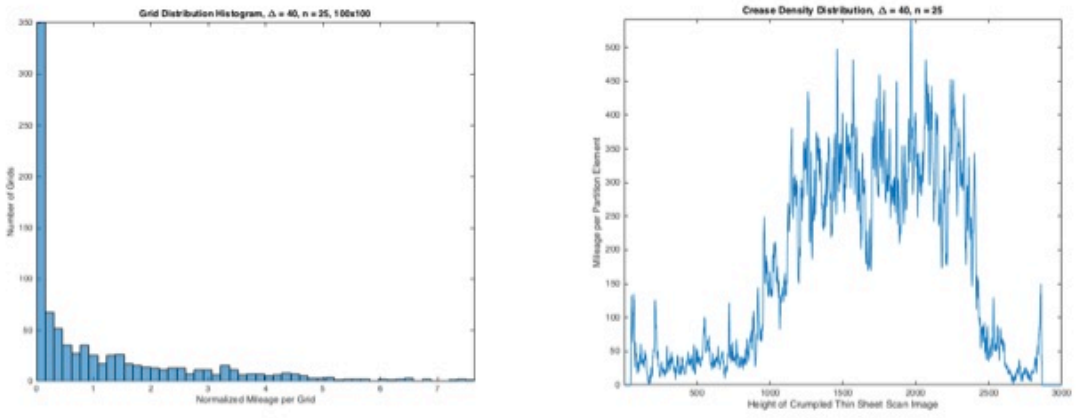

Figure A-2. Crease density distributions for (Δ = 0.63,* n *= 25). *Representative figures used for analysis of crease density distributions. (a) The histogram of grid element mileages, in millimeters, for grid size 100x100. (b) The horizontal element mileages as a function of the height of the element in the crumpled sheet scan.*

The third mode of image analysis used in this thesis is the Hough transform, a feature detection technique that is used to find the location and orientation of shapes in an image (Ballard, 1981). The Hough transform first plots various lines at different angles through each data point in the original space, then plots a line perpendicular to the above-mentioned lines through the origin, and finally, measures the distance (r) and angle (θ) of each perpendicular line. This associates a set of (r, θ) coordinates for each point in the original space; the graph of this set of coordinates in the Hough space, defined by (r, θ) coordinates, represents the output of the Hough transform for the desired point. The (r, θ) curves associated with collinear points in the original space will intersect in the Hough space; thus we can identify lines from the original space as the intersection peaks in the Hough space. Each such peak corresponds to a (r, θ) value; the θ value allows us to determine the angles corresponding to the creases on our crumpled sheet. An example of an original sheet scan and the corresponding Hough space can be seen in Figure A-3(a) and (b). We perform the Hough transform in MATLAB using the 'hough' function. To determine the frequencies of lines of certain angles, we sum the square of the peak values associated with each angle in the Hough transform and compare the sums; a representative frequency graph can be seen in Figure A-3(c).

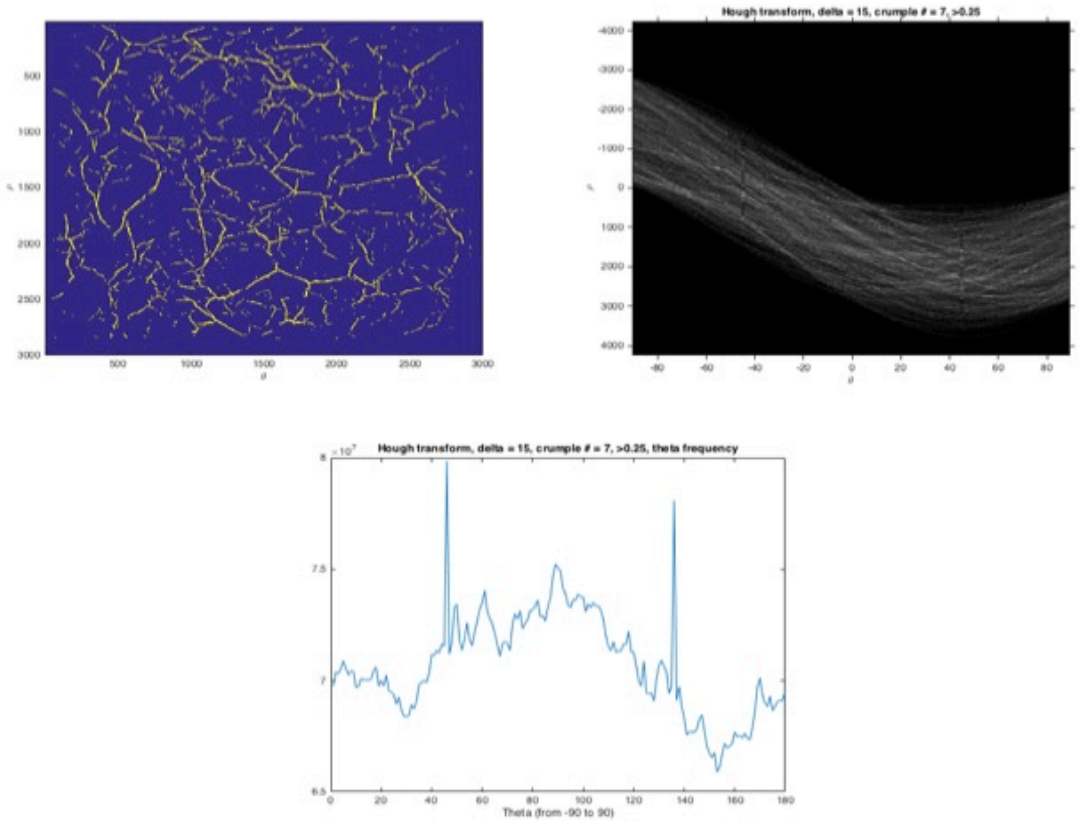

Figure A-3. Hough transform analysis for (Δ = 0.18,* n *= 7). *Image analysis with the Hough transform to determine the directionality of creases. (a) Filtration of the crumpled sheet scan to highlight the valley creases. (b) The Hough space, with coordinates (r, θ) corresponding to the valleys shown in A-3(a). (c) The frequency of line intersection in A-3(b) for each angle; peaks correspond to the most common angles of creases in Figure A-3(a).*

Section A.3 Laser Profilometer

We use the profilometer scans of the crease structure of the crumpled sheet created by Omer Gottesman. The profilometer laser is shined to produce a vertical line of light onto the crumpled sheet, while a camera captures the intersection between the light and the surface of the sheet; from the side, the brightness of a point corresponds to the height of the sheet (Blair and Kudrolli, 2005). By imaging in this manner across the entire width of the crumpled sheet, the profilometer constructs a contour map of the sheet surface. We

then use a trigonometry-based algorithm to determine the curvatures of the height contours displayed on the scan image, thus converting the contour network of the scan image into a network of crease valleys and ridges. Positive curvature corresponds to the crease valleys; negative curvature corresponds to the crease ridges.

Section A.4 Yoshimura Pattern

Yoshimura buckling, which we examine more closely in Appendix C, is defined by the triangular mesh pattern that appears on thin cylinders under axial loads (Yoshimura, 1955; Hoff, 1966). While the Yoshimura mesh pattern is uniform and easy to identify in purposely folded origami cylinders, as seen in Figure A-4(a), their identification, measurement, and characterization are more difficult in uncontrolled and disordered systems. We attempt to quantify the effect of Yoshimura buckling in our crumpled thin sheets by counting the number of diamonds (comprised of two adjacent triangular mesh elements) in a crease network and by measuring the width of these diamonds; an example of our identification method can be seen in Figure A-4(b). We recognize the crudeness of this methodology, as well as the potential for uncertainty; we believe that further exploration of the Yoshimura pattern in crumpled thin sheets with cylindrical shape memory would be valuable.

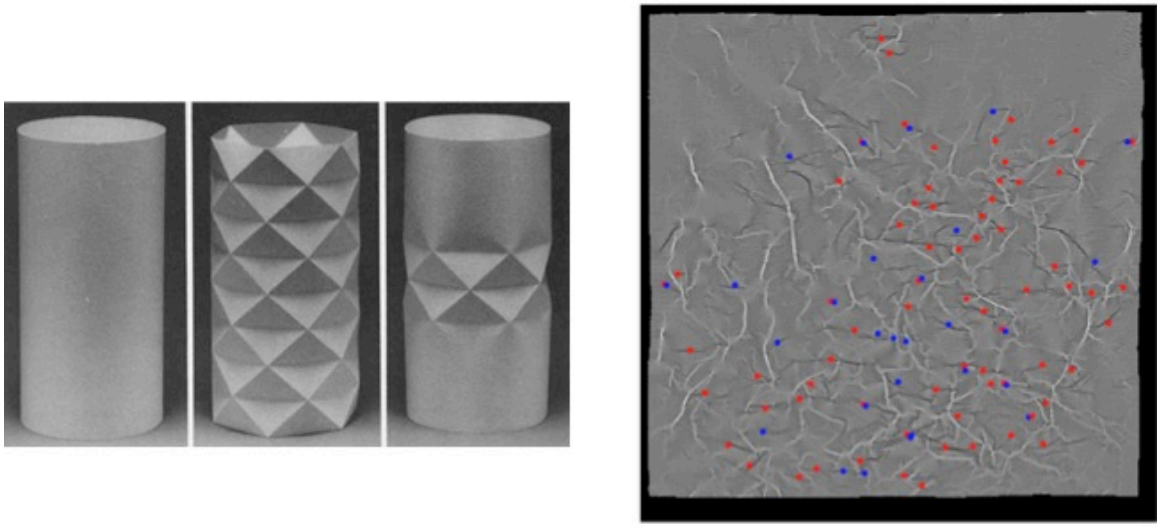

Figure A-4. Yoshimura buckling. *The triangular Yoshimura mesh pattern contributes to buckling in thin-wall cylinders. (a) The Yoshimura pattern in a thin-walled cylinder, made via origami (image from Tarnai, 1997). (b) Identification of Yoshimura diamonds (two adjacent mesh triangles connected by a horizontal folding line) in a scan of a crumpled sheet with (*$\Delta = 0.45$, n *= 10). Red dots indicate crease patterns identified as definite Yoshimura diamonds; blue dots indicate uncertain diamonds; dots with both blue and red indicate probable diamonds.*

Appendix B. Memory and Directionality of Creases

Section B.1 Introduction

In Chapter 5, we explored the crease density distribution as a means to understanding how the characteristics of the crease structure, besides mileage, affect the memory capacity of a crumpled sheet. One of the other variables that we attempt to quantify and study is the directionality of creases, i.e., the angles of the defects. In this section, we discuss the details and results of our efforts in that regard.

We investigate the directionality of creases by using the relative frequency of defects of certain angles. We want to see if, for example, a given crumpled sheet has a greater

percentage of creases at 45° angles than another sheet (all angles are denoted from the normal). We model the relative frequency of a crease angle as the ratio of the frequency of that angle to the median of the frequencies of all angles. Further, we wish to determine if the frequency ratio changes for crumpled sheets with the same mileage but different radii, in order to evaluate the impact of crease directionality on memory.

Section B.2 Experimental Method and Results

To determine the directionality of the creases of a crumpled thin sheet, we utilize the Hough transform (see Appendix A.2) to analyze the profilometer scans (see Appendix A.3) of crumpled thin sheets produced by Gottesman. By examining the regions of the Hough space with the greatest frequency of line intersection, we can correspondingly find the angles that appear most often in the crease structures of crumpled sheets.

We examine the valleys and ridges for a set of scans with the same mileage, but different (Δ, n) values, focusing on creases with θ = -45°, 0°, 45°. These numbers were chosen due to the prominence of scars at these angles both in the Hough space and on the crumpled sheet scans. Further, their presence in the Yoshimura pattern (see Appendix C) is suggestive of their ability of these creases to affect the memory capacity of a crumpled thin sheet. The relative frequency of valleys with θ = -45°, 0°, 45° are shown in the figures below, with relative frequency defined as the ratio of the frequency of the creases of angle θ and the mean frequency of creases of all angles.

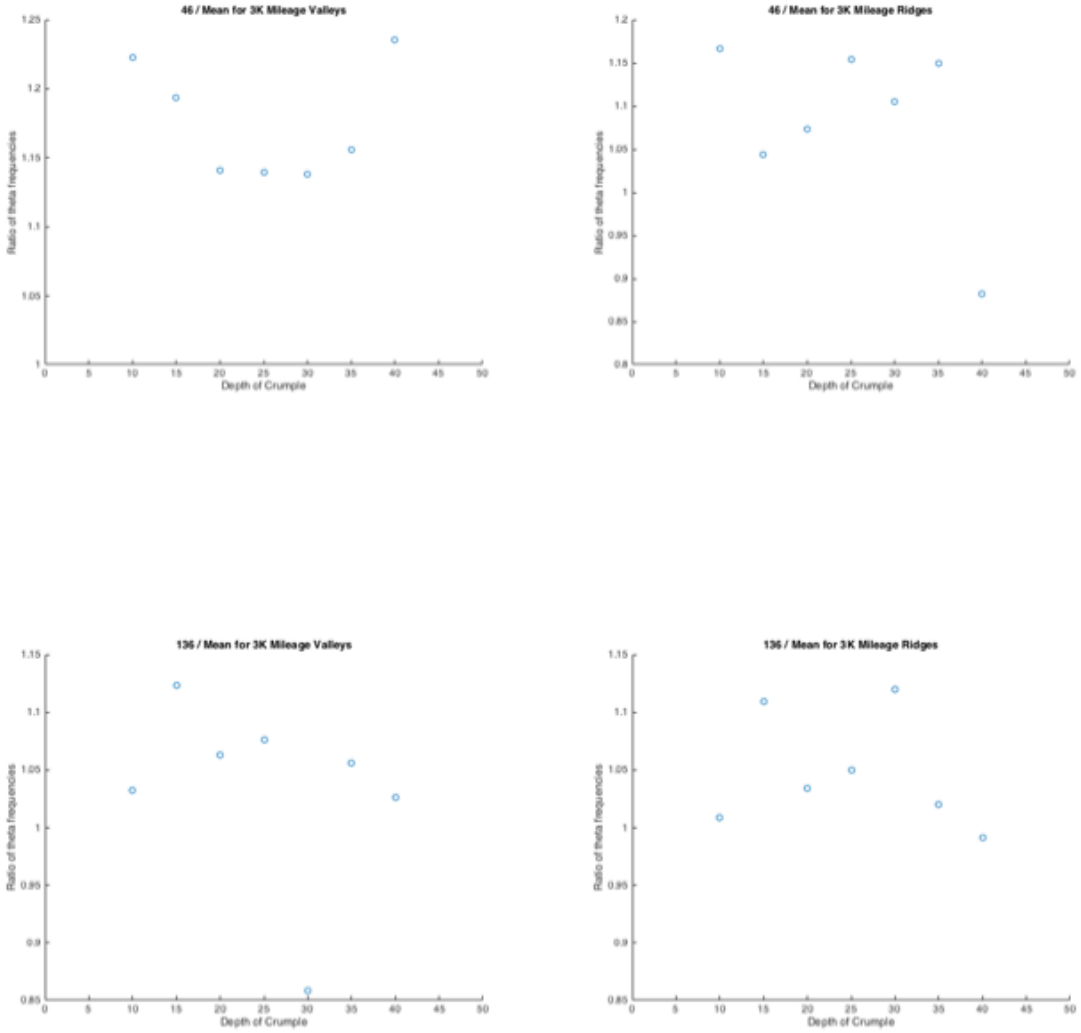

Figure B-1. Relative frequency of creases for crumpled sheets of 2.4k mileage. *The ratio of the frequency of defects at θ = ±45° to the mean frequency for all θ, for Δ values ranging from 0.045 to 0.63. (a) The ratios of θ = -45° for the 'valley' creases. (b) The ratios for θ = -45° for the 'ridge' creases. (c) The ratios of θ = 45° for the 'valley' creases. (d) The ratios of θ = 45° for the 'ridge' creases.*

Section B.3 Discussion

We see no pattern in either of the figures above, suggesting a lack of correlation between the relative frequency of creases at the three angles examined and the retained radius in a

crumpled thin sheet. A greater proportion of angles at -45° or 45° correlates with neither an increase nor a decrease in the memory capacity of a thin sheet; the same holds for horizontal creases (i.e., angle creases of 0°). It remains a possibility that directionality lines has an impact on radius, though not at the angles examined; the relative frequency of other crease angles may effect the retained radius. Unfortunately, it was not possible to accurately record the relative frequencies of creases with angles of -90° or 90° due to noise in the Hough transform extraction from the crumpled sheet edges. In addition, it is also possible that the Hough transform, as used here, was unable to accurately capture the information that we sought, especially given our unfamiliarity and inexperience with the technique.

Interestingly, there is an increase in the absolute frequency of creases with θ = 45°, 0°, 45°. It appears that a greater number of crumples leads to more creases at certain angles, but not a higher percentage of those creases, suggesting that there are, in general, more scars produced by increasing n, which matches the results found in Gottesman and summarized earlier in Chapter 3 and 4.

Section B.4 Conclusion

In this chapter, we have attempted to isolate the directionality of the creases in a crumpled sheet and examined the effect of directionality on the retained radius of curvature. Using the Hough transform, we determine the relative frequencies of creases at angles -45°, 0°, 45° for crumpled thin sheets for l = 2.4k; however, these frequencies did not vary with the radius of curvature. We therefore are unable to conclude that changes to

the relative frequency of crease angles affect the memory capacity of a crumpled thin sheet, although uncertainties in both our methodology and our results exist.

Appendix C. Yoshimura Buckling

As alluded to in Appendix A.4, Yoshimura buckling is a mesh pattern that appears in thin-walled cylinders undergoing axial loads. The mesh pattern, comprised of isosceles triangles, allows for the cylinder to buckle and compress as the load increases (Yoshimura, 1955). Though the buckling pattern is developable, the cylinder undergoes deformation and vertex and edge movement as the object collapses under greater loads.

We conjecture that Yoshimura buckling might be present in our crumpled thin sheets, given the imposition of a cylindrical shape in our protocol. This is supported by our analysis of the crease network scans, in which we are able to see the characteristic combination of oblique fold lines, horizontal fold lines, peaks, and flattened triangular shapes of the Yoshimura pattern (de Vries, 2005). We want to see if the presence of the Yoshimura pattern has any effect on memory retention in the crumpled sheets; to quantify the presence of the mesh pattern, we count the number of 'diamonds,' which we define as two adjacent triangle mesh elements connected by a horizontal fold line, and measure the width of each diamond for a set of scans of the same l but different (Δ, n) values. The number of diamonds and the diamond widths are shown as a function of Δ in Figures C-1 and C-2.

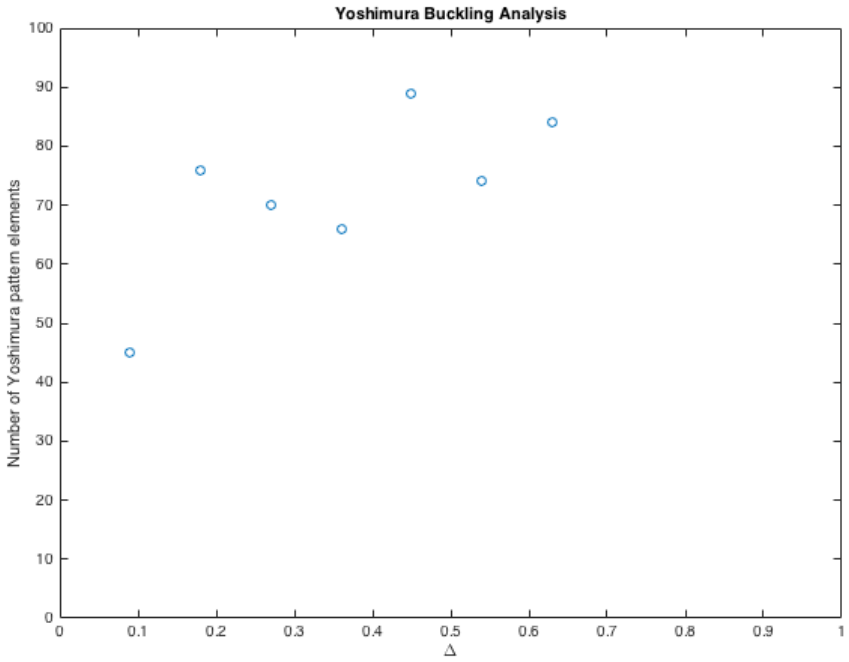

Figure C-1. Yoshimura pattern element count. *The number of Yoshimura pattern 'diamonds' identified from the crumpled sheet scans for l = 2.4k, for Δ values ranging from 0.09 to 0.63.*

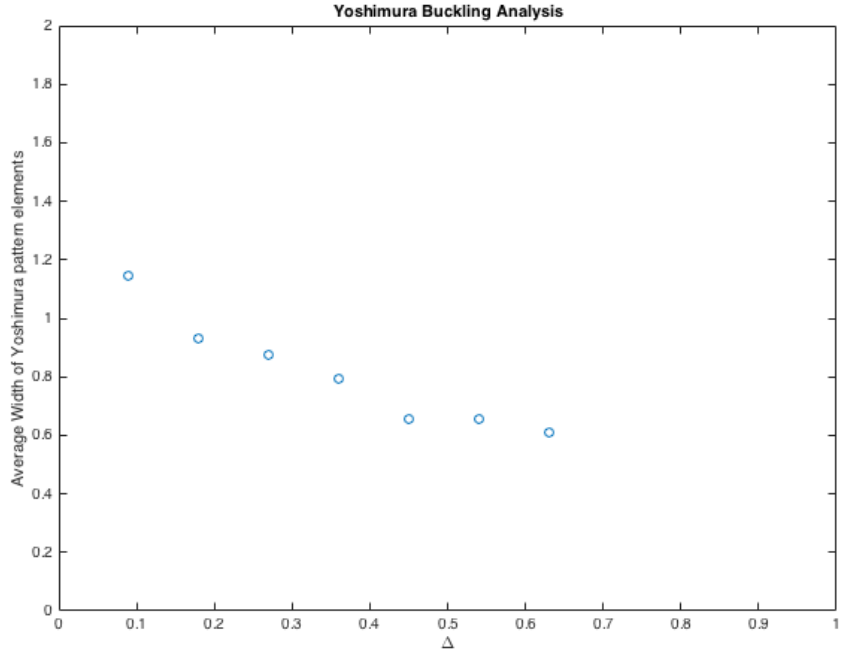

Figure C-2. Yoshimura pattern element width. *The average width of Yoshimura pattern 'diamonds' identified from the crumpled sheet scans for l = 2.4k, for Δ values ranging*

from 0.09 to 0.63. The diamond widths were measured by ruler and are in units of centimeters.

One caveat in interpreting the data shown in Figures C-1 and C-2 is that there is great uncertainty due to the small sample size and the unscientific nature of our identification and width measurement of the Yoshimura pattern elements, which were done entirely by hand. Based on our results, we are unable to draw any conclusions on a relationship between Δ and the number of Yoshimura 'diamonds,' though there appears to be a tenuous upward trend in the number of diamonds for larger Δ values. On the other hand, Figure C-2 shows a clear relationship between the average width of the diamonds and Δ: it suggests that the width of the diamonds decreases as Δ (and n) increases, with an R^2-value of 0.976 for the exponential fit,

$$y = 0.8463 * e^{-3.375*x} + 0.5089.$$

This matches our results from Chapter 5, where we saw that the combination of shallow depth of crumple and high number of crumples resulted in densely packed crease structures. Similarly, a low average width value for the Yoshimura diamond elements suggests a high density of the Yoshimura mesh in high (Δ, n) sheets. Though we would again emphasize the uncertainty in this analysis of Yoshimura buckling in crumpled sheets, it is not difficult to conjecture a link between greater density in crease structure and narrower Yoshimura diamonds. Such a relationship could help explain the greater retention of radius of curvature that we see in shallow crumple, high n sheets, given the association between buckled cylinders and the Yoshimura mesh. It is possible that Yoshimura buckling could provide a physical explanation for the mechanism of shape retention in crumpled thin sheets—or, perhaps, it is simply one explanation among many.